Design of a Novel Cancer Suicide Gene Therapy Regulated by Casein Kinase II (CK2)

A

Thesis

Presented to

the faculty of the School of Engineering and Applied Science

University of Virginia

---

in partial fulfillment

of the requirements for the degree

Master of Science

by

Logan Campbell

December 2023

APPROVAL SHEET

This

Thesis

is submitted in partial fulfillment of the requirements
for the degree of

Master of Science

Author: Logan Campbell

This Thesis has been read and approved by the examing committee:

Advisor: Matthew Lazzara, Ph.D.

Advisor:

Committee Member: Silvia Blemker, Ph.D.

Committee Member: Bryan Berger, Ph.D.

Committee Member:

Committee Member:

Committee Member:

Committee Member:

Accepted for the School of Engineering and Applied Science:

Jennifer L. West, School of Engineering and Applied Science

December 2023

ACKNOWLEDGEMENTS

This thesis was supported by my incredible partner, family, friends, and colleagues. I want to thank my advisor, Matt Lazzara, for his guidance, mentorship, and unwavering support throughout my time at UVA. I would also like to thank the members of the Lazzara lab for their unwavering support and for building a great environment in which to work. I would also like to extend my thanks to the many great collaborators with whom I have been able to work. I am also very grateful for the opportunities that study at UVA has granted, especially the Biotechnology Training Program. Lastly, I want to thank my partner, Iona, for her endless support and love during my journey at UVA.

ABSTRACT

Viral vectors have long been pursued as attractive potential alternatives or adjuvants for chemotherapy-resistant cancers. A major focus of that work has been the development of retroviral vectors for suicide genes that encode non-mammalian enzymes capable of converting innocuous prodrugs into cytotoxic metabolites. Suicide gene therapies have thus far failed to reach the clinic despite more than two decades of clinical trials, which we hypothesize have involved inherently flawed vector designs that rely on either weak, cancer-specific promoters or strong, non-specific viral promoters. We previously designed a new suicide gene vector that overcomes this efficacy-limiting tradeoff by combining a strong viral promoter with a posttranslational cancer stability switch based on the activity of the oncogenic extracellular signal-regulated kinase (ERK) pathway. In that design, a suicide gene (herpes simplex virus thymidine kinase or yeast cytosine deaminase) was fused with a nuclear localization sequence and an unstable PEST domain (rich in proline, glutamic acid, serine, and threonine) from the FRA1 transcription factor, which is stabilized when phosphorylated by ERK. In this thesis, we sought to extend the success of that design by creating a suicide gene product stabilized by casein kinase II (CK2), a holoenzyme with constitute activity that is widely involved in disease progression and chemoresistance in cancers including glioblastoma. The major challenge in designing a CK2-regulated suicide gene is that PEST-like peptide sequences regulated specifically by CK2 are unknown. To address this, we implemented a two-stage design process beginning first with a small panel of peptide sequences based primarily on a FRA1 scaffold with incorporation of CK2 phosphorylation sites. The peptide sequences were intentionally designed to capture variation in properties including the number and strength of PEST domains and CK2 phosphorylation motifs, as well as the positioning of these along the peptide. FLAG-tagged fusions of these peptide sequences with herpes simplex virus thymidine kinase were stably expressed in glioblastoma cells and evaluated for their stability and response (degradation) to

CK2 pharmacological inhibition. Because the most CK2-regulated peptide was also the least stably expressed, a machine learning model was constructed to predict the peptide features that most determine peptide stability. Based on the model, a second-generation of the most CK2-regulated peptide was engineered and found to have superior stability while retaining strong regulation by CK2 activity. Specificity of the second-generation suicide gene product for regulation by the two CK2α catalytic subunits was confirmed using stable shRNA-mediated knockdowns. Furthermore, we found that the second-generation suicide gene product was stabilized in its expression in response to the chemotherapeutic carboplatin in a CK2-dependent manner and that carboplatin and GCV synergistically killed glioblastoma cells engineered to express the suicide gene. Thus, this work produced a novel cancer suicide gene vector engineered for specific regulation by a kinase that is broadly important in disease progression and therapeutic resistance and provides a framework for the deployment of machine learning algorithms to design other kinase-regulated suicide genes in an iterative fashion.

TABLE OF CONTENTS

LIST OF TABLES

LIST OF FIGURES

CHAPTER 1: INTRODUCTION

1.1 SUICIDE GENE THERAPY

Overview

Suicide gene therapy (SGT) is an innovative approach to target cancer through the introduction of exogenous genetic materials into cells. Unlike many other types of gene therapy, this approach does not involve introducing correct versions of a gene or knocking out a deleterious gene. Instead, the gene introduced encodes an enzyme that converts an innocuous prodrug into a cytotoxic product that causes apoptosis in targeted cells. To function effectively and avoid off-target effects, the expression of the introduced gene is often controlled by some oncogenic characteristic specific to the cancer being targeted. This results in selective expression in cancer cells and, ideally, low to no expression in healthy cells. Due to this differential expression, the cancer cells are primed to respond to a prodrug and eventually apoptosis if the system works optimally. Despite the intelligent design of these systems, none have been adopted for clinical use, but SGTs are still being actively investigated for cancers such as glioblastoma (GBM).

Key components and mechanism of action

The key components of an SGT are the delivery system, prodrug-converting enzyme, and the mechanism of achieving selectivity. Many of these systems have historically relied on viral gene delivery to a target site. Multiple modalities of viral packaging have been applied, with adenoviral delivery being the most frequently used in clinical trials (NCT03603405, NCT01913106, NCT02831933, NCT03541928, NCT00844623, NCT03596086, NCT00002824, NCT00870181, NCT02894944). Retroviral and lentiviral packaging systems are alternative methods to deliver a gene that convey distinct advantages[1,2].

Lentiviral and retroviral methods cause integration of the delivered genetic material into the host cell genome, which results in long-term expression but can lead to off-target effects[1]. These lentiviral and retroviral systems can also carry a larger payload, permitting more complex vector designs. AAV-based delivery is highly effective at infecting target cells but does not result in integration into the genome and is more limited in payload size[1,3]. Additionally, retroviruses can only infect actively dividing cells, which may endow selectivity for rapidly dividing cancer cells but does limit delivery efficiency and could miss senescent cancer cells[1].

There are multiple options for the encoded prodrug-converting enzymes. The herpes simplex virus thymidine kinase (HSVtk) or gamma cytosine deaminase (γCD) are most frequently used[4]. These enzymes use different prodrugs and slightly different mechanisms to kill cancer cells, but the basic mechanism of action is similar. The most notable difference is in the bystander effect, an effect where cells expressing the SGT can induce cell death in neighboring uninfected cancer cells. The γCD system achieves a superior bystander effect compared to HSVtk because it can release toxic products into the microenvironment while the HSVtk system requires junctions between cells[2,4]. Whether a strong bystander effect is desired would greatly depend on the targeted cancer environment and concern over specificity.

Lastly, achieving cancer selectivity has multiple points of potential regulation that might limit off-target effects. To date, most clinical trials have relied on cancer cell proliferation and intratumoral injection to confer selectivity with replication-incompetent adenoviral vectors (NCT03603405, NCT01913106, NCT02831933, NCT03541928, NCT00844623, NCT03596086, NCT00002824, NCT00870181, NCT02894944). While this location- and replication-based targeting has been the primary approach, many preclinical studies have been performed that offer a more refined mechanism through transcriptional targeting. These approaches have placed expression of the suicide gene under promoters that are overactive in cancer[1]. Some of the overactive promoters tested thus far include hTERT, Cox2, FOS, E2F1, and ERBB2[2]. A Phase I trial of an ERBB2 promoter-driven suicide gene was tested for breast cancer already

and demonstrated high selectivity, but reductions in tumor volume were limited, and no follow-up studies were conducted[5]. Transcriptional targeting has recently been clinically tested with oncolytic virus-based therapies using the hTERT promoter for conditional viral replication (NCT03190824, NCT03172819, NCT03921021). Preclinical and early-stage trials have indicated that these approaches yield high safety and efficacy in targeting tumors[6,7]. However, sufficient expression for therapeutic levels of a suicide gene is a frequent concern for transcriptionally targeted approaches[8]. Recently, an alternative approach was introduced that achieves selectivity through post-translational regulation of the suicide gene protein, with high efficacy demonstrated *in vitro* and *in vivo*[9]. In this design, a protein stability switch stabilized by oncogenic ERK activity is fused to a suicide gene. This results in a suicide gene protein that accumulates in cells with high ERK activity and is rapidly depleted in cells with low ERK activity. Selectivity can be achieved through multiple mechanisms, and the method chosen can determine expression and cancer specificity.

Each design decision can alter key attributes, sometimes at the cost of others; however, the optimal product will have a high accumulation of the prodrug-converting enzyme (HSVtk, γCD) present selectively in tumor cells. This makes these cells susceptible to a prodrug that, upon administration, should lead to rapid cell death in these primed cells while sparing healthy cells. Optimally, this cell death will also stimulate an immune response toward the whole tumor.

Physical delivery methods

Most clinical trials and proposed applications of this technology have been delivered via direct intratumoral injection, and many of these trials have been focused on treating glioblastoma (GBM) (NCT03603405, NCT03596086, NCT00002824, NCT00870181, NCT01156584). GBM poses a more difficult delivery obstacle than most locations. Since GBM is a type of brain cancer, delivery of a viral SGT is limited by anatomical barriers such as the blood-brain barrier and the skull. Historically, delivery methods have been restricted to intensive

surgical procedures to inject the virus intracranially or in the post-resection cavity[10]. This approach is not optimal due to the potential safety risks of brain surgery, invasiveness, limited practitioners, and expense for the patient. There is investigation into less invasive technologies, such as focused ultrasound. This method would allow intravenous delivery of the SGT and passage through the blood-brain barrier via a temporary opening[11]. This method would also benefit from a different delivery system, such as cationic microbubbles, which could enhance transduction efficiency. Delivery of these therapies is one of the most significant limitations, and further research could enable them to be more viable treatments.

Clinical trials

Thus far, clinical trials have not demonstrated the efficacy of SGTs, but they have indicated high safety. Over a dozen phase I/II trials have been conducted, but only two phase III trials for this method have taken place[4]. Two products using an HSVtk system reached late-stage trials. Most notably, in a phase III trial in 2000, an HSVtk system was applied to 248 patients with primary GBM[4,12]. This demonstrated high safety, but there was no increase in survival or prolongation of progression-free survival when the gene was encoded in fibroblasts that were implanted near the target tumor[4]. More recently, the now-dissolved company Tocagen tested a γCD system in a replication-competent retrovirus called Toca 511, which also reached phase III trials for GBM and astrocytoma[13]. Despite promising results in early-stages, this late-stage trial did not meet primary endpoints, nor did it extend survival when compared to standard care treatments[13]. However, there are still companies pursuing this method of treating brain cancer. Currently, three trials are using the HSVtk system (NCT01811992, NCT03596086, NCT03603405), and future studies will likely include alternative DNA-delivery methods (e.g., lipid nanoparticles), alternative tumor delivery, and combinations with chemotherapies or immune therapies.

1.2 GLIOBLASTOMA

Overview

Glioblastoma is a relatively rare form of cancer, affecting approximately 3.2 individuals per 100,000[14]. Despite its rarity, GBM stands out as the most prevalent primary malignant cancer of the brain and central nervous system[15]. Originating from various cell types, particularly those with neural stem-cell properties[16], GBM typically occurs in older individuals, with a median age of onset at 64 years. However, cases can manifest at any age and are more frequently observed in men. It is important to note that primary cases of GBM, as opposed to secondary cases, carry a poorer prognosis[14]. GBM has one of the lowest survival rates among all cancers, with fewer than 5% of patients surviving beyond five years following diagnosis[14]. Without treatment, the median survival is a mere three months. Even with standard treatments, such as surgical resection, chemotherapy with temozolomide (TMZ), and radiation, the median survival extends only to 14 months[15].

Current treatment methods

The treatment approach for GBM involves a combination of surgical resection, radiotherapy, and chemotherapy. Achieving complete surgical resection is challenging due to the tumor's location in areas of high functional importance and its propensity for invasiveness. The standard treatment regimen after surgery combines radiotherapy and TMZ[15]. TMZ, a DNA alkylating agent, induces methylation of guanine residues, disrupting replication and leading to cell cycle arrest at the G2/M phase, followed by apoptosis[17]. However, more than 50% of GBM patients fail to respond to TMZ, and others rapidly develop resistance, often associated with O6-methylguanine-DNA methyltransferase (MGMT)[15]. The high degree of plasticity and heterogeneity in GBM cells further complicates treatment. Overall, treatment options are limited, and, even when aggressively applied, they fail to improve patient outcomes markedly.

Genetic and signaling differences in GBM

Primary GBM cases have complicated genetic profiles, often associated with loss of heterozygosity (LOH) in chromosome 10 (approximately 60-80% of cases)[17]. These cases exhibit a myriad of heterogeneous alterations that frequently impact crucial pathways such as p53, receptor tyrosine kinase/Ras/PI3K, DNA damage repair, and the retinoblastoma pathway (Rb)[15,17]. The alteration of these critical pathways contributes to enhanced cell proliferation, survival, checkpoint evasion, and drug resistance.

One of the most frequently observed mutations in GBM occurs in the epidermal growth factor receptor (EGFR)[18]. These mutations often involve amplification in EGFR expression or the expression of a mutated form, EGFRvIII. EGFR amplification leads to overactivation of downstream pathways, such as Ras, enhancing proliferation, altering cellular development, and promoting tumor migration[19]. The mutated form, EGFRvIII, is truncated and present in approximately 30% of cases[19]. This mutant lacks the extracellular binding domain, resulting in constitutive activation and stimulating pro-survival signaling to a higher degree, aiding in resistance to chemotherapies[17,18].

Other alterations affecting downstream signaling, particularly in the MAPK pathway, are also frequent[18]. Deletion of neurofibromin 1 (NF1) is commonly observed in GBM, as well as in other neoplasms[18]. NF1 acts as a negative regulator of Ras, allowing further enhanced activation of downstream targets. Additionally, alterations are frequently observed in the potent PI3K-AKT pro-survival signaling pathway through mutation of the tumor suppressor gene phosphatase tensin homology (PTEN) in primary GBM[17,18]. PTEN negatively regulates PI3K activation through dephosphorylation of PIP3, suppressing pro-survival and proliferative signals; thus, mutations in this gene lead to enhanced signaling through AKT. Numerous other alterations are present in GBM, providing further advantages that allow these tumors to escape treatment, rapidly spread, and adapt.

Future treatment opportunities

Despite significant research efforts, GBM remains challenging to treat due to intratumoral heterogeneity, blood-brain barrier penetration issues, cellular plasticity, and drug resistance. Ongoing clinical trials explore combinations of standard care with monoclonal antibodies, engineered viruses, targeted inhibitors, CAR T-cells, and additional chemotherapy drugs[15]. Suicide gene therapies, while showing promise in preclinical studies, have not yet realized their potential in clinical trials. Over fifteen clinical trials testing suicide gene vectors for GBM have demonstrated safety but did not improve outcomes[1]. The untapped potential of suicide gene therapies emphasizes the need for future developments enabling selective targeting to enhance treatment outcomes.

1.3 CASEIN KINASE II (CK2)

Overview

Casein kinase II (CK2) is a holoenzyme encoded by three distinct genes for two catalytic subunits (α/α') and a catalytically inactive regulatory unit (β)[20]. As a constitutively active kinase, CK2 exhibits extensive pleiotropy, influencing many cellular targets and participating in a myriad of cellular processes. Although CK2 is not a prototypical oncogene, cancer cells showcase a peculiar addiction to CK2 due to its involvement in proliferation, pro-survival signaling, alterations in cancer metabolism, and heightened capacity for DNA damage repair[21]. This dependency has prompted the development of various CK2 inhibitors, with several undergoing clinical trials as both monotherapies and combination treatments.

CK2 structure and regulation

CK2 exhibits the unique ability to function as catalytically active monomers (α/α') or as a tetramer composed of two catalytic subunits and two regulatory β subunits[20]. Interaction with the β regulatory subunit modulates substrate targeting and can enhance activity toward some targets but prevent interaction with others[20,22]. CK2 substrates are divided into three subclasses. Type I substrates can be phosphorylated by catalytic monomers or by the tetramer and are the most common; type II substrates are targeted solely by the CK2α/α' subunits, and Type III substrates are exclusively targeted by the CK2 tetramer[22]. In general, CK2 targets acidic regions and requires a minimum consensus sequence of [S/T]-X-X-[D/E] to target substrates.

Regulation of CK2 expression is poorly understood, and as a constitutively active kinase, regulation of its activity is not well characterized. CK2 demonstrates self-regulation through multiple methods, including post-translation modifications (PTMs) and protein-protein interactions. Post-translationally, CK2 can autophosphorylate itself in either catalytic or regulatory subunits, enhancing activity and preventing proteasomal degradation[20]. Protein-protein interactions with other CK2 subunits can increase activity and alter their expression through negative feedback. An overabundance of either α or β subunits results in negative intrinsic regulation aimed to equalize stoichiometries between catalytic and regulatory units[20]. However, CK2 can also be regulated by extrinsic proteins through similar mechanisms. Src-family kinases are known to phosphorylate CK2α, which leads to up to three-fold increases in activity[23]. Additionally, CK2 activity can differ throughout the cell cycle. For example, phosphorylation of CK2 by a key enzyme in cell cycle regulation (Protein kinase C) enhances catalytic activity[24]. Overall, while the regulation of CK2 is yet to be well defined, it appears that much of its regulation is self-mediated, but extrinsic signaling can also alter expression or activity.

CK2 in cancer and interaction with signaling pathways

CK2 exhibits prevalent overexpression and heightened activity in various cancers, including hematological malignancies, brain tumors, breast cancer, colon cancer, ovarian cancer, and pancreatic cancer[25]. Within GBM specifically, dosage gains have been observed in greater than 30% of GBM samples for CK2α catalytic subunits[26]. The overexpression and overactivation of CK2 are generally associated with worse prognosis in most cancer types[25]. This is unsurprising as cancer cells have demonstrated a higher dependence on CK2 signaling than healthy cells and the range of pathways that CK2 signaling affects[29].

CK2 activity affects many cellular pathways through hundreds of targets, with documented targets affecting nearly 25% of the phospho-proteome[22,27]. Many of these substrates are transcription factors, proteins involved in DNA repair, and signal proteins involved in proliferation and cell survival[28]. Given this broad coverage and high involvement in key processes, it is not surprising that alterations in CK2 signaling could provide an advantage to cancer cells.

Support of cell survival and apoptosis evasion are key mechanisms by which CK2 promotes tumorigenicity. Multiple pathways, including PI3K/AKT and IKK/NFkB, are amplified, and heat shock protein (HSP) chaperone machinery is supported by CK2. These, in turn, support cell survival[26,29]. CK2 upregulates the PI3K/AKT pathway at multiple nodes. First, CK2 phosphorylates AKT, which induces more activity, and secondly, CK2 downregulates PTEN, a negative regulator of this pathway[26,29]. This multi-factored mechanism results in strong survival signaling. CK2 also promotes the degradation of IKK, which enhances NFkB. Active NFkB then translocates to the nucleus, increasing pro-survival gene expression[26,29]. Another way CK2 promotes survival is through the prevention of apoptosis. CK2 phosphorylates multiple targets within the apoptotic program, preventing caspase activation and protecting substrates from caspase-mediated cleavage[30]. Together, these activities support pro-survival signaling and make cells with overactive CK2 more challenging to treat.

Beyond pro-survival signaling, CK2 regulates other pathways that promote antitumor drug resistance. CK2 is heavily involved in many types of DNA damage repair and supports a multi-drug resistance (MDR) phenotype. CK2 directly promotes DNA repair by enhancing the activity of proteins involved in repairing single-strand breaks (SSBs) through XRCC1 and double-strand breaks (DSBs) through XRCC4, MDC1, and MRE11[27,29]. Beyond enhancing these DNA damage repair activities, CK2 supports multi-drug resistance phenotypes through increasing drug efflux. CK2 phosphorylation of MRP1, an efflux pump, has been shown to increase the efflux of chemotherapies, with CK2 knockdowns leading to high intracellular drug accumulation[29]. CK2 also phosphorylates and induces the overexpression of another efflux pump, P-gp, which further enhances drug resistance through decreased intracellular drug accumulation[29]. Together, CK2 activity supporting these mechanisms can severely impact antitumor drug efficacy.

CK2 as a therapeutic target

CK2's upregulation in multiple cancer types and widespread involvement in a litany of signaling pathways upregulated in cancer have made it an attractive target for treatment. The drug furthest along in development is silmitasertib (CX-4945), an ATP-competitive small molecule inhibitor of CK2 catalytic subunits. There are multiple ongoing or completed clinical trials testing silmitasertib for cancer. These include a Phase I study targeting refractory myeloma (NCT01199718), Phase II studies targeting basal cell carcinoma (NCT03897036) and recurrent medulloblastoma (NCT03904862). In addition, the combination of silmitasertib with cisplatin and gemcitabine for cholangiocarcinoma is currently being tested in Phase II trials (NCT02128282). Additionally, multiple preclinical studies have been conducted using chemotherapy in combination with CK2 inhibition. Results from these have demonstrated CK2 inhibition displays strong synergism with cisplatin, carboplatin, and gemcitabine in ovarian and cholangiocarcinoma and ovarian cancer cell lines[31,32]. Synergism has also been observed in

glioblastoma models when silmitasertib is combined with temozolomide[33,34]. These studies and CK2's involvement in many survival and drug resistance pathways highlight the potential of targeting CK2 in many forms of cancer.

1.4 PROTEIN ENGINEERING

Overview

Protein engineering methods have rapidly expanded over the past few decades, enabling the development of novel biologic drugs. Historically, protein engineering has applied rational engineering methodology or directed evolution to guide the modification of native proteins for altered activity or new properties[35]. These approaches were applied to rationally or randomly alter specific residues and were both time-consuming and required a high degree of expertise[36]. More recently, the toolbox for protein engineering has expanded to enable more targeted alterations, *de novo* designs, and has become more accessible[36]. Breakthroughs in machine learning methods have vastly accelerated this advancement, and artificial intelligence is expected to lead to further breakthroughs[37]. Protein engineering has been critical for biologic drugs, with even fully *de novo* designs now being tested in clinics[38,39] and will likely continue to drive novel treatments.

Computational methods for protein structure prediction

Prediction of protein structures from amino acid sequences has rapidly evolved in recent years and has attracted high interest for the rational engineering of novel proteins. These advances have been enabled through the accumulation of large structural repositories, enhanced computing power, and the development of machine learning algorithms. Structures are predicted through template-based modeling (TBM), in which closely aligned structural data exists, or template-free modeling (TFM)[40,41]. TFM uses molecular dynamics simulations to find

the lowest energy conformation and assumes these low energy conformations would be native structures[41]. Previously, TFM methods had low accuracy; however, deep learning methods have vastly improved, enabling complex fragment-based assemblies and molecular dynamics simulations[41]. One of the most promising fronts is the end-to-end modeling of proteins from just sequence alone, which allows deep neural network models to produce 3D structures without running computationally exhaustive folding simulations[42]. However, these models fail to predict structures for intrinsically disordered proteins or regions (IDP/IDRs)[43,44]. Much of the proteome contains completely disordered proteins or disordered regions, which do not adopt stable structures[45]. An issue with predicting the structural properties of these regions is their incompatibility with protein crystallization techniques. This is probably due to IDRs adopting transient structures that can be rapidly altered[46]. However, understanding these regions' structural properties is needed as they display high functional importance through facilitating protein-protein, protein-DNA, and protein-RNA interactions.

Protein phosphorylation and kinase targeting prediction

While traditional protein engineering has been focused on site-directed mutagenesis, post-translational modifications can vastly alter protein properties. Specifically, protein phosphorylation plays an essential role in modulating protein functions and ensuring proper cell functioning. These post-translational modifications (PTMs) can alter protein activity, folding, stability, and subcellular localization[47]. Due to these important functions, large databases that catalog experimentally validated phosphorylation sites have been constructed. There are hundreds of thousands of documented sites across multiple organisms, and the number is steadily increasing[48]. However, experimental studies to document these sites are costly and slow, leading to the development of models to predict new phospho-sites using machine learning. Thus far, approximately 40 computational methods have been developed to predict these interactions using protein sequence, structure, functional features, or a combination of

these[49]. However, an evaluation performed on a subset of these tools has found much poorer accuracy when evaluating test datasets than reported in their original publications[48]. Another limitation of these tools is their coverage of kinases. While many of the phospho-sites have been documented, there is limited knowledge of kinases responsible or functional role of these PTMs[50].

A notable advancement in predicting kinases responsible for phosphorylation was recently published by Dr. Lewis Cantley's lab at Cornell[51]. In this work, they developed a model to predict kinase-substrate interactions from protein sequence alone. This was achieved through screening synthetic peptide libraries to determine substrate specificity for over 300 kinases to determine sequence motifs associated with each kinase. This tool could effectively help close the gap between the large number of annotated phospho-sites and the kinases that target these sites. This tool does not lend insight to the structural or functional effects of phosphorylation, but it could be used a valuable resource to engineer peptides for phosphorylation by targeted kinases and to evaluate potential off-target regulation by alternative kinases.

CHAPTER 2: DESIGN AND EVALUATION OF A SUICIDE GENE THERAPY REGULATED BY CK2

2.1 ABSTRACT

Suicide gene therapies (SGTs) are a promising, investigational mode of cancer treatment in which cancer cells are transduced to express exogenous enzymes that convert innocuous prodrugs into cytotoxic metabolites. We propose that the failure of SGTs to succeed beyond Phase III clinical trials is related to their mechanisms of expression and selectivity for cancer cells. We previously demonstrated the efficacy of an alternative approach for specific SGT expression wherein the benefits of strong viral promoters can be combined with a post-translational stability switch controlled by the oncogenic kinase ERK. In that design, fusion of the suicide gene encoding herpes simplex virus thymidine kinase (HSVtk) with the PEST domain of the FRA1 transcription factor, which is stabilized when phosphorylated by ERK, creates a novel SGT that specifically sensitizes cells to prodrug-mediated cytotoxicity in high-ERK cancer cell environments. Here, we sought to extend the success of that ERK-regulated design to create an SGT stabilized by casein kinase II (CK2), an important kinase involved in cancer cell survival across oncology but without known substrates with phosphorylation-induced stabilization. To engineer a PEST-like peptide domain regulated specifically by CK2, we undertook a two-stage design process. We first engineered a small library of six PEST domains based primarily on a FRA1 backbone which included sequences displaying CK2 consensus phosphorylation motifs and PEST domains of varying strengths. Each SGT vector was used to stably transduce a glioblastoma cell line, and the resulting panel of cell lines was used to evaluate the CK2-dependent stabilization of the novel HSVtk fusions in response to the CK2 inhibitor CX-4945. Using the stability data as a dependent variable and biochemical or sequence-based features (e.g., C-terminal PEST instability scores) as independent variables,

we created a machine learning model to identify the peptide characteristics that most strongly control SGT stability. Insights from this model guided the engineering of a second-generation SGT variant with improved stability that retains high CK2 specificity. We validated this variant for CK2-specificity and activity-dependent stability using a combination of small-molecule inhibition and RNA interference approaches. We further demonstrated the ability of this SGT to induce cancer cell death in a CK2-dependent manner in response to the prodrug ganciclovir and the cooperativity of the second-generation SGT with the carboplatin due to a CK2-dependent SGT stabilization in response to the chemotherapeutic. In addition to generating a novel CK2-regulated SGT, this work blueprints an approach that can be used in the future for the rational engineering of other oncogenic kinase-stabilized SGTs.

2.2 INTRODUCTION

Cancer has conventionally been treated with chemotherapeutics that preferentially cause damage to the most rapidly dividing cells. This approach is effective in some settings, but it is highly non-specific and leads to transient and long-term side effects in non-transformed cells leading to the well-known side effects of hair loss and severe nausea but also to less frequently discussed serious impairments in fertility and cognitive function. In many cases, even initially responsive cancers develop chemoresistance mechanisms. These factors have led to a high interest in targeted therapies for cancer, which leverage the overexpression or amplification of proteins that participate in oncogenesis and disease progression. Targeted approaches are often based on small molecule drugs designed to bind and inhibit overactive kinases crucial to cancer growth and survival. The precision of these drugs generally reduces side effects and results in improved outcomes in a variety of cancers. In virtually all cases though, small molecule drugs that are initially effective become ineffective due to resistance mechanisms that

arise through mutation or bypass signaling[52-54], motivating a need to design alternative pathway-specific modes of cancer therapy.

Suicide gene therapies offer a promising and highly selective approach to cancer treatment. They involve two critical steps: first, the introduction of DNA to cells that encodes an exogenous enzyme usually delivered via a viral vector, and second, the treatment of these cells with non-toxic prodrugs that the enzyme converts into cytotoxic agents[55]. SGTs provide several advantages over conventional cancer treatments, as they can be tailored for cancer-specificity. Thus far, most clinical trials have used delivery location and cancer cell proliferation to achieve SGT cancer specificity (NCT03603405, NCT01913106, NCT02831933, NCT03541928, NCT00844623), but simple modifications to the vector design can permit more precise targeting. This precise selectivity can be achieved using tumor-specific promoters such as hTERT, COX2, FOS, E2F1, and ERBB2[1,56,57]. However, few of these methods have been tested in clinical trials, and there are concerns about whether they can drive sufficient expression for therapeutic efficacy[8]. SGTs offer another advantage by exhibiting a bystander effect, enabling cells expressing an SGT to extend their cytotoxic impact to neighboring non-transduced cancer cells through the diffusion of activated prodrugs or transport via gap junctions[2,58,59]. Despite their promise and unique advantages to current treatments, SGTs have not yet advanced to clinical use.

In a previous study, our laboratory reported an innovative strategy to achieve an alternate mode of achieving cancer selectivity with high gene expression by utilizing the cytomegalovirus (CMV) promoter in conjunction with a post-translational stability switch regulated by the oncogenic kinase ERK[9]. In this design, the suicide gene herpes simplex virus thymidine kinase (HSVtk) or yeast cytosine deaminase was fused to the C-terminal PEST domain of the FRA1 transcription factor, which had previously been used to create a live-cell ERK reporter[60]. This domain is stabilized when phosphorylated by ERK at two serine residues (S252, S265), resulting in a SGT whose expression is controlled by the activity of oncogenic

ERK[9,60]. The FRA1 PEST motif was used as the molecular switch because its protein degradation is promoted when it is unphosphorylated[61].

Typically, PEST regions are recognized as signals for protein degradation and are rich in proline (P), serine (S), aspartic acid (E), and threonine (T), which are commonly found in short-lived proteins[62,63]. These PEST motifs are frequently found within intrinsically disordered protein regions (IDRs) and enhance local disorder, although their exact mechanism in protein degradation remains unclear[64]. Regions of high protein disorder can promote ubiquitin-dependent or -independent proteasomal degradation[65]. Lastly, physical insights into these PEST domains within IDRs can be challenging due to their inability to be crystallized and examined using traditional protein structure analysis approaches[45]. We sought to determine if native PEST domains could be leveraged as scaffolds to build new protein stability switches for SGTs regulated by oncogenic kinases other than ERK. This study is focused on constructing a novel PEST-containing SGT regulated by casein kinase II (CK2).

CK2, a constitutively active serine/threonine kinase, is frequently overexpressed in various cancer types, including glioblastoma and cervical cancer[25]. CK2 comprises three subunits, including the CK2α and CK2α' catalytic units and the CK2β regulatory subunit. Interestingly, CK2α and CK2α' can function independently of CK2β or associate as a holoenzyme composed of two CK2α/α' subunits and one CK2β subunit, which can alter substrate specificity and increase activity[20]. Despite being ubiquitously expressed, cancer cells rely on CK2 for survival, leading to the concept of them being “addicted” to CK2[21]. CK2's distinctiveness lies in its impact on the phosphoproteome, affecting over 700 known substrates and representing up to 25% of the phospho-proteome[22,27,66]. This broad influence results in alterations to key signaling pathways, such as IKK/NFkB, JAK2/STAT3, Wnt/β-catenin, PI3K/AKT, DNA repair, and multi-drug resistance drug efflux, ultimately promoting enhanced proliferation, improved survival, and drug resistance[21,25,28]. Given CK2's pivotal role in these pathways, there is a growing interest in developing CK2 inhibitors for cancer therapy. For

example, the CK2 inhibitor silmitasertib (CX-4945) is currently under investigation in clinical trials, both as a monotherapy and in combination with other treatments for various cancer types (Trials: NCT03904862, NCT02128282, NCT03571438, NCT03897036). Because of the broad relevance of CK2 in oncology, we chose to develop a novel SGT that is selectively stabilized by CK2 activity.

To design a CK2-regulated SGT, we first constructed a small library of candidate peptides that were predicted to be phosphorylated by CK2. We then constructed a machine learning model to identify the sequence-based features that most impact the stability of CK2-specific regulation of the peptides. Model inferences were used to engineer a second-generation peptide with enhanced stability and CK2 specificity. Fusion of the second-generation peptide with HSVtk created a highly CK2-selective SGT that cooperates with carboplatin for enhanced killing of glioblastoma cells via a carboplatin-induced stabilization of the fusion protein. The development of this new pipeline for engineering novel kinase-regulated SGTs will enable the design of alternative kinase-regulated SGTs and other fusion proteins where kinase-mediated stabilization is useful.

2.3 MATERIALS AND METHODS

Computational methods

Protein sequence-based feature generation.

Peptide sequence-based information was generated from the five FRA1-based fusion protein variants, excluding the Novel PEST variant. The Novel PEST variant was excluded because it was not based upon the FRA1 scaffold. Physicochemical parameters of the entire FRA1-based inserts were calculated using the ExPASY ProtParam module[67] and PEST measurements were calculated using ePestfind webtool[68]. The number of CK2 sites was calculated as sequences present on each variant conforming CK2 minimal consensus sequence

[S/T]-X-X-[D/E]. Additional C-terminal features were generated by aligning the variants following a shared 'SPTE' CK2 consensus site present on all FRA1-based inserts. The ProtParam and ePESTfind webtools were also used on these C-terminal domains to calculate the region's instability index, terminal PEST scores, isoelectric point. Additionally, positional features were generated by considering the proximity of the closest and second closest CK2 consensus site to the C-terminus.

PLSR modeling to relate sequence-based features to fusion protein stability

Protein stability was determined based on immunoblot-based measurements of the FLAG-tagged fusion protein normalized by co-expressed GFP of each variant. The average measurement for each variant was used as a vector of outcomes (Y) for the PLSR model. The protein sequence-based features were used to create a matrix of independent variables (X). Model generation and feature selection were performed in R using the *ropls* package. Leave-one-out cross-validation was applied to determine model performance, and 500 permutations were applied to the predictor set to generate the null distribution to determine the significance of model performance on a basis of Q^2Y. Model refinement was performed by retaining features from the initial full model with a VIP score > 1. This reduced feature set was used to generate a final PLSR model and guide the design of a fusion protein that retains selective regulation by CK2 but with increased stability.

Experimental methods

Cell culture and reagents

U87MG cells expressing EGFRvIII (Dr. Frank Furnari, PMID: 20133782) were maintained as adherent cultures in DMEM (Thermo Scientific, 11-965-092) containing 10% FBS (Avantor, 97068-085), 1mM L-glutamine (Gibco, A2916801), 100 units/mL penicillin (Thermo, 15140122), and 100 µg/mL streptomycin (Thermo, 15140122). Cells were maintained at low

passage numbers and tested for mycoplasma using MycoAlert PLUS Detection Kit (Lonza). Cells were grown in a Thermo Scientific Forma Steri-Cycle i160 incubator at 5% CO_2 and 37°C.

Plasmids and cloning

A pMSCV-IRES-GFP retroviral vector backbone (Dr. Dario Vignali, Addgene plasmid # 52107) engineered to encode FLAG-tagged HSVtk[9] was used as the starting point to create CK2-regulated fusion proteins. The PEST-domain variants encoding predicted CK2-regulated domains were fused to HSVtk through restriction digest of pMSCV immediately downstream of HSVtk-FLAG and ligated to geneBlocks (Twist Biosciences) encoding inserts with compatible sites. Final versions of these products were verified through whole-plasmid sequencing (Primoridium Labs). Oligonucleotides for short hairpin RNAs targeting CK2α and CK2α' were cloned in pLKO.1-puro (Dr. Bob Weinberg, Addgene plasmid # 52107). Two targeting sequences were validated for each CK2 catalytic subunit. CK2α was silenced with shRNAs targeting the UTR (target sequence: 5'-ATTACCTGCAGGTGGAATATT-3') region or coding region (target sequence: 5'-GCCATCAACATCACAAATAAT-3'). CK2α' was also silenced with two shRNA targeting the UTR (target sequence: 5'-ATCAAACCTCACTTCCGAATG-3) or coding region (target sequence: 5'-CTGGGACAACATTCACGGAAA-3'). A non-target vector was used as a control in shRNA-mediated knockdown experiments (target sequence: 5'-GCGCGATAGCGCTAATAATTT-3').

Virus production and cellular selection

Retroviral particles containing the HSVtk-PEST/IRES-GFP cassette were produced by calcium phosphate-mediated transfection of amphitropic Phoenix 293T cells (Dr. Gary Nolan, Stanford University). Virus was harvested and filtered through a 0.45 μm PVDF membrane at 24 and 48 hr after transfection. Fresh virus was immediately delivered to target cells in two infections supplemented with polybrene (1 μg/mL). Cells were then selected by fluorescence-

activated cell sorting (FACS) on a FACSAria Fusion cell sorter (BD Biosciences) by staff of the UVA Flow Cytometry Core facility. Lentivirus encoding shRNA sequences were produced through cationic lipid-aided (FuGENE6) co-transfection of LentiX 293T cells (Lonza) with the pLKO.1 lentiviral vector and packaging vectors (pCMV-VSVg, pDelta8.2). Virus was harvested and filtered 48 hr post-transfection and directly applied to target cells supplemented with polybrene. Cells were selected in 2 μg/mL puromycin for three days and maintained in 1μg/mL puromycin.

Inhibitors, therapeutic molecules, and antibiotics

CK2 inhibitors CX-4945 (MedChemExpress HY-50855) and DMAT (ApexBio A3368), ganciclovir (ApexBio B209), temozolomide (Santa Cruz Biotechnology, sc-203292A), and carboplatin (Santa Cruz Biotechnology sc-202093A) were reconstituted at manufacturer-recommended dilutions in DMSO.

Antibodies

Monoclonal antibodies against CK2α (sc-373894) and CK2α' (sc-514403) were purchased from Santa Cruz Biotechnology. Antibodies against FLAG (#8146), pAKT (S473, #9271), ERK (# 4695), GAPDH (#2118), γH2AX (S139, #9718), and GFP (#2555) were purchased from Cell Signaling Technologies. Secondary antibodies for immunofluorescence imaging were conjugated to Alexa Fluor 546 or 647 (Life Technologies). Infrared dye-conjugated secondary antibodies for immunoblotting were purchased from Rockland Immunochemicals (anti-mouse IgG IRDye700 conjugated, 610-130-121; anti-rabbit IgG DyLight800 conjugated, 611-145-002).

Western blotting

Whole-cell lysates were prepared using a standard cell extraction buffer (Invitrogen, FN0011) with protease and phosphatase inhibitors (Sigma-Aldrich P8340, P5725, P0044). Crude lysates were centrifuged at ~20,800 rcf for 10 min, and the clarified supernatant total protein concentration was quantified using a BCA assay. Equal amounts of protein were loaded with DTT, 4× LDS sample buffer, and ultrapure water and denatured for 10 min at 100°C. Samples were loaded on 15-well NuPAGE gradient (4-12%) gels. Following electrophoresis, gel contents were transferred to 0.2 µM nitrocellulose membrane using the TransBlot Turbo Transfer System (BioRad). Membranes were blocked for 1 hr in Intercept Blocking Buffer (IBB, LI-COR) on a shaker at room temperature. Primary antibodies were diluted in IBB and incubated with the membrane overnight at 4°C on an orbital shaker. Membranes were washed three times with PBS-Tween (0.1% Tween) and then incubated with secondary antibodies diluted 1:10,000 in IBB for 2 hr. Following three PBS-Tween washes after secondary staining, membranes were imaged on a LI-COR Odyssey. Following PBS-Tween washes, membranes were imaged on a LI-COR Odyssey. Immunoblot band intensities were quantified using Image Studio software (LI-COR) and measurements were normalized by loading control (LI-COR). If required for membrane re-staining, membranes were stripped using 0.2M NaOH and were subsequently stained using the same procedure mentioned above.

Immunofluorescence staining and imaging

Cells were plated on glass coverslips in 6-well dishes for small-scale experiments at densities of 150,000 cells per well for experiments shorter than 3 days. For larger scale experiments, cells were plated in 96-well plates at a density of 8000 cells per well for short term experiments (< 3 days) and 4000 cells per well for longer experiments (~ 5 days). Cells were fixed in 4% paraformaldehyde for 20 min and permeabilized with PBS-0.25% Triton X-100 for 3 min. Following permeabilization, cells were incubated with primary antibodies diluted in IBB at manufacturer suggested concentrations overnight at 4°C. Following five washes in PBS-Tween

(0.1% Tween), conjugated secondary antibodies and Hoechst nuclear stain were diluted in IBB and applied to cells. Cells were incubated with secondary antibodies for 1 hour at room temperature and washed five times in PBS-Tween (Coverslip-mounted samples were imaged using a Zeiss AxioObserver Z1 widefield microscope with a 10 or 20× objective and Axiocam 506 digital camera. 96-well samples were imaged using a Cytation5 (BioTek) with 10 or 20× objectives. For coverslip-mounted samples, at least three fields of view were imaged per biological replicate. For 96-well samples, at least 4 fields of view were imaged per replicate. Identical exposure times and image settings were used across replicates for each combination of imaging platform and plating format.

Image analysis of fluorescence microscopy

Automated image quantification was performed using pipelines constructed in CellProfiler v4.2.1 (Broad Institute). Primary objects were identified using Hoechst nuclear staining, and whole-cell domains were identified as secondary objects using GFP or ERK staining. Cellular measurements of FLAG fluorescent intensity were normalized by GFP intensity to quantify differences in fusion protein stability on an equal-transduction basis. Where reported, nuclear-to-cytoplasmic ratios were quantified by dividing the mean nuclear fluorescence intensity by the mean cytoplasmic intensity of a per cell basis. Measurements of intensities on a per cell basis were exported as comma spaced variables and analyzed in R.

Flow cytometry for cell death quantification

For cell death experiments, cells were plated in 6-well plates, and cell treatments were performed as described in figure legends. At the conclusion of experiments, floating and adherent cells were collected, resuspended in PBS containing TO-PRO-3 (Life Technologies, 1:10,000), and stored on ice until analysis. Within an hour of collection, cells were analyzed for TO-PRO-3 permeability with a FACSCalibur cytometer (BD Biosciences). Data collected from

flow cytometry experiments was analyzed in R using the *FlowCore, ggCyto,* and *OpenCyto* packages.

2.4 RESULTS

Retroviral vector encoding FLAG-tagged HSVtk fusion proteins and a panel of peptides designed for CK2 regulation

Previously, our lab developed an ERK-regulated suicide gene by fusing FLAG-tagged HSVtk to the C-terminal FRA1 PEST domain. In this study, we sought to develop an analogous regulatory domain controlled by CK2 phosphorylation. Lacking a known endogenous substrate whose stability is specifically regulated by CK2-mediated phosphorylation, we began by designing a small library of six peptides that we predicted would be regulated by CK2. Five of the six were based on the FRA1 PEST domain as a scaffold. In each of the designs based on FRA1, the ERK phosphorylation and docking sites were removed.

The CK2 regulatory domains of each fusion protein had differences in the number of CK2 consensus motifs ([S/T]-X-X-[D/E]), motif compositions (residues n+1 and n+2), affinity of each motif for CK2 phosphorylation, the distance of the sites from the protein C-terminus, the number of PEST domains, and the strength of PEST domains (Fig. 1A). The PEST domains were designed to have different numbers and strengths of PEST motifs, which were identified and scored using the EMBOSS ePestfind webtool[68], which combines the local enrichment of proline (P), glutamic acid (E), serine (S), and threonine with a hydrophobicity term. Positive PEST scores are generally associated with short half-lives or sites of potential proteolytic cleavage[62]. Affinities were scored using the Kinase Library tool (Supp. Table 2)[51]. We included sites encompassing a range of affinities because previous studies have shown that even when CK2 is genetically or chemically inhibited, it retains basal activity sufficient to drive substrate phosphorylation[69]. We believed that too tight of an interaction could slow the dynamic rate of phosphorylation and dephosphorylation.

All FRA1-based sequences included one conserved CK2 consensus sequence (SPTE), which is predicted to have low affinity for both CK2 catalytic subunits (α/α'). Every FRA1-based variant, excluding FRA1-CAM, has CK2 motifs clustered solely in the C-terminus (Fig. 1A, Supp. Table 1). The FRA1-CK2, FRA1-CK2.2, and FRA1-stCK2 are highly similar, each containing three PEST domains, but the number of CK2 motifs and PEST domain strengths differs (Supp. Table 1). FRA1 and FRA1-stCK2 include four CK2 motifs, each with two high-affinity and one low-affinity CK2 motif (Supp. Table 2). FRA1-stCK2 was engineered to have a stronger PEST domain in the N-terminus of the regulatory peptide (Fig. 1A). FRA1-CK2.2 differs by having six CK2 motifs (five high-affinity, one low-affinity) but contains relatively similar PEST domain strengths as FRA1-CK2 (Supp. Table 2). The FRA1-AKT variant only contains two PEST domains and two CK2 motifs that are predicted to have weaker CK2 affinity (Fig. 1A, Supp. Table 1 & 2). The more C-terminal CK2 motif includes a segment of 10 residues from human AKT1, which CK2 natively targets[70]. FRA1-CAM includes five high-affinity CK2 motifs that are well distributed across the whole sequence and include two strong PEST domains. Lastly, the Novel PEST does not use FRA1 as a scaffold and represents a *de novo* design constructed to maximize PEST domain coverage and strength. This variant includes two strong PEST domains and two high affinity CK2 sites (Fig. 1A, Supp. Table 1 & 2).

Each of the six peptides described was fused to FLAG-tagged HSVtk and cloned into a retroviral vector (pMSCV) with the expression cassette under the control of a strong CMV viral promoter and with an IRES-EGFP co-expression element (Fig. 1B). FLAG was included for easy detection because HSVtk antibodies are not readily available. pMSCV vectors encoding the fusion protein variants were used to package retrovirus, and U87MG glioblastoma cells were engineered with stable SGT expression. The resultant transductants were flow-sorted to retain only GFP-positive cells.

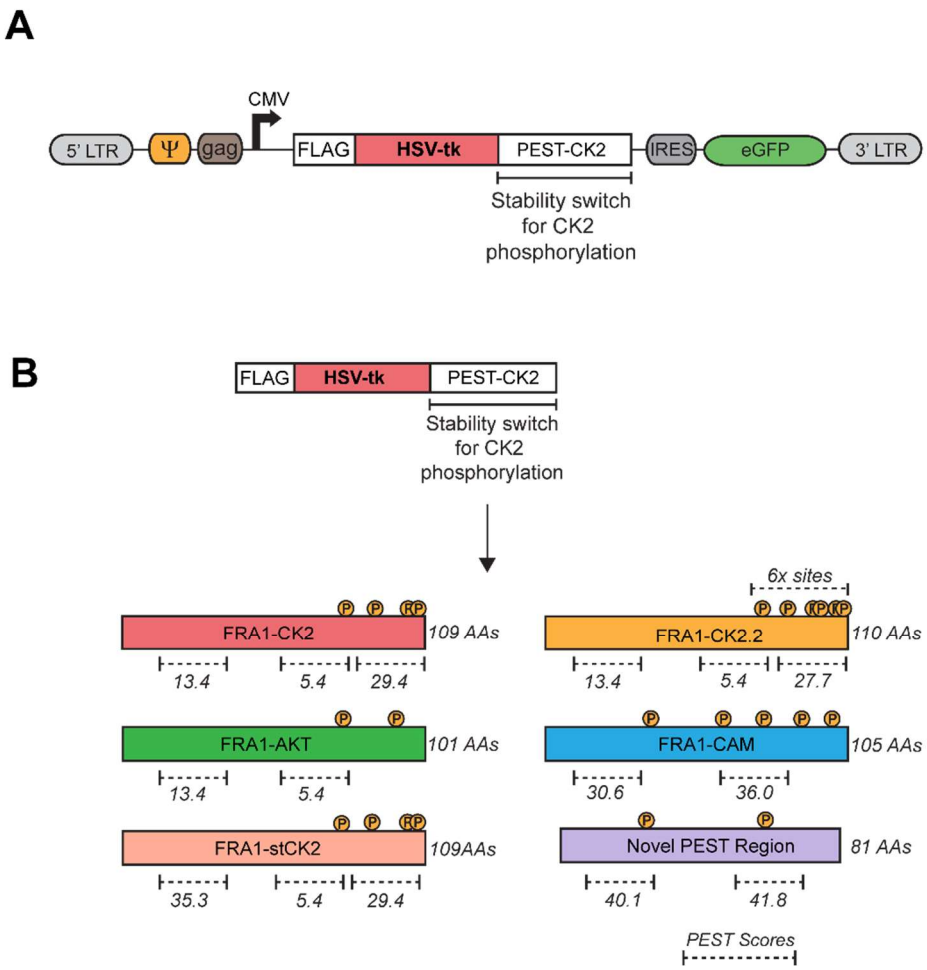

Fig. 1: Schematic of vector composition and fusion proteins designed for regulation by CK2. (A) Domain diagram of the expression cassette showing the FLAG-tagged HSVtk fused to stability regulatory domains designed to be phosphorylated by CK2, followed by EGFP under an internal ribosomal entry site (IRES). (B) Schematics of five FRA1-based regulatory domains and one *de novo* domain (Novel PEST) designed for regulation by CK2 displaying differences in the number of PEST domains, PEST scores for those domains, CK2 phosphorylation motifs, and overall length.

Evaluation of HSVtk fusion protein stability and CK2 sensitivity

To assess the stability and CK2-mediated regulation of the peptides we designed, we measured the expression of FLAG-tagged HSVtk fusion proteins in transduced U87MG cells by immunoblot and immunofluorescent imaging following inhibition. Substantial variation in expression was observed across the fusion protein variants (Fig. 2A). The FRA1-AKT fusion displayed the lowest accumulation of all variants, with significantly less signal than all other

FRA1-based constructs (FRA1-CK2, FRA1-CK2.2, and FRA1-stCK2) and the novel construct (Novel PEST) (Fig. 2A). The CAM-CK2 variant was significantly lower than FRA1-CK2, FRA1-stCK2, and Novel PEST constructs (Fig. 2A). Next, we examined whether and to what extent the fusion proteins responded to CK2 inhibition as a measure of the ability of CK2 to stabilize the fusion proteins. In transduced U87MG cells expressing HSVtk fusion proteins treated with 10 μM of the CK2 inhibitor CX-4945 (silmitasertib) or DMSO as a control, immunofluorescence and image analysis for FLAG revealed that only one of the six fusion protein variants, FRA1-AKT, was depleted in response to CK2 inhibition (Fig. 2B). Another variant (FRA1-stCK2) displayed a significant enhancement in accumulation due to CK2 inhibition (Fig. 2B). Our objective was to uncover if any variants were depleted due to lessened CK2 activity, which could indicate that the SGT stability was modulated by CK2-mediated phosphorylation. Only one variant, FRA1-AKT, displayed this characteristic and was chosen as the top candidate for a CK2-regulated SGT. Notably, the FRA1-AKT construct also exhibited the lowest baseline accumulation (Fig. 2A), which we aimed to improve to enhance the cytotoxic potential of the SGT.

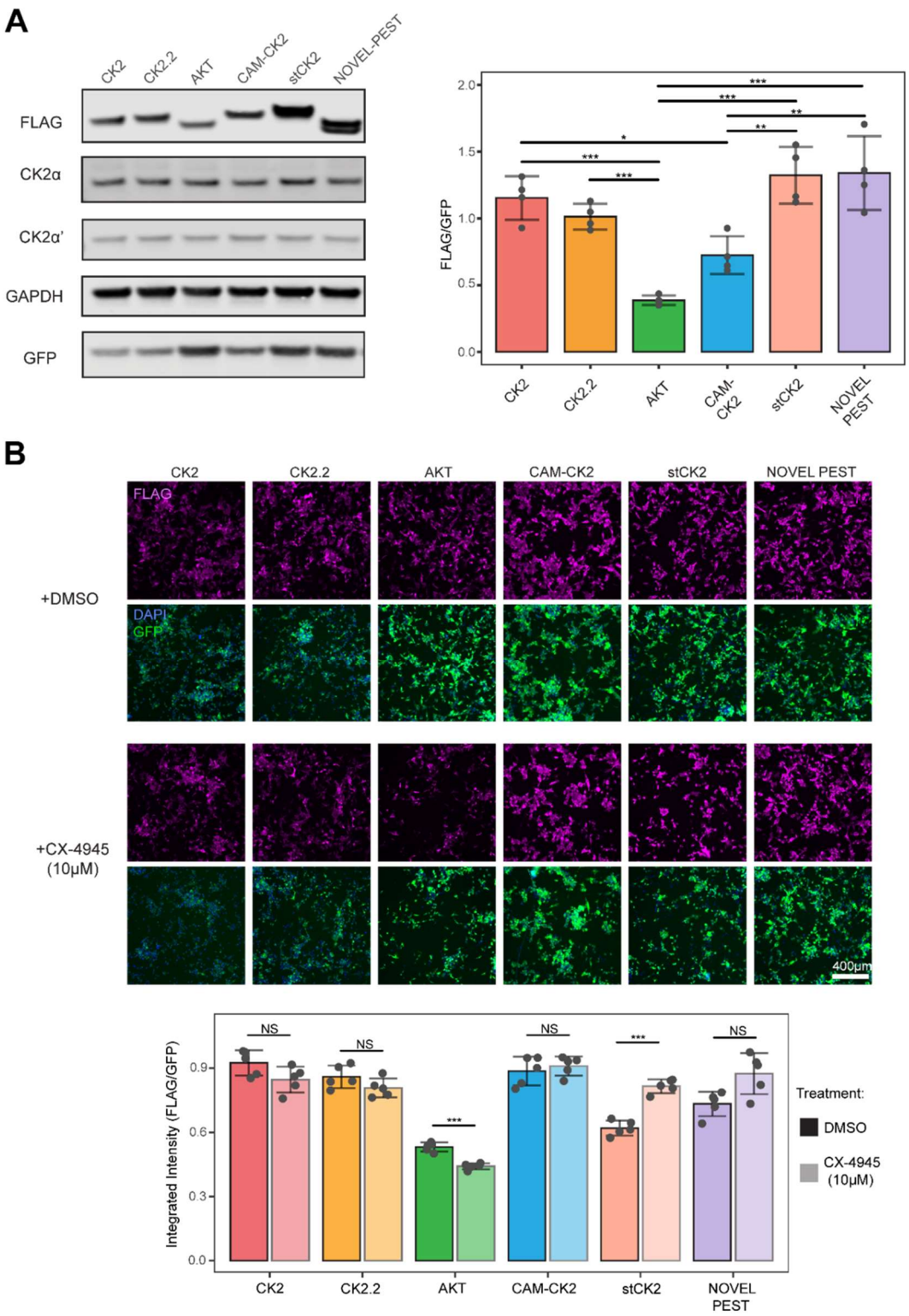

Fig. 2: Evaluation of intracellular stability and CK2 responsiveness of a panel of potential CK2-regulated fusion protein designs. (A) U87MG cells stably expressing FLAG-tagged SGT variants and GFP under an IRES were lysed and subjected to immunoblotting using the indicated antibodies to examine baseline expression. Densitometry was used to quantify the GFP-normalized FLAG signal. Image is representative of n = 4 replicates, and data are plotted as mean

± sd. A one-way ANOVA and Tukey post hoc test were applied to determine the significance of observed differences; *, **, and *** indicate p = 0.05, 0.01, or 0.001, respectively. (B) The transduced U87MG cells were treated for 24 hr with the CK2 inhibitor CX-4945 (10 μM) or DMSO and then fixed prior to immunofluorescence microscopy for FLAG and GFP expression. The GFP-normalized FLAG signal intensity was quantified per cell. Images are representative of five biological replicates, with four fields of view per replicate. Data are displayed as mean ± sd. A Student's t test was applied to determine the significance of the indicated differences; *, **, and *** indicate p = 0.05, 0.01, or 0.001, respectively.

Data-driven modeling to identify stability-enhancing features

Given the low stability of the FRA1-AKT fusion protein, we undertook a systematic approach to identify the peptide features that regulate stability, with the goal of rationally designing a second generation FRA1-AKT construct with enhanced stability while retaining CK2 sensitivity. This led us to build a partial least squares regression (PLSR) machine learning model based on features of the regulatory domains to predict intracellular stability. We generated features based on protein sequence, position of CK2 consensus sites (ex. distance to C-terminus), and physicochemical properties of each FRA1-based regulatory domain as predictors (**X, 9 features**, Table 1, Supp. Table 3) of intracellular stability (**Y, 5 observations**) obtained from untreated samples (Fig. 1C). PLSR was selected as it is well-suited to datasets containing more features than independent conditions or observations of a system. We also decided to exclude the Novel PEST variant as it poorly aligned with all FRA1-based variants, which would be the basis of the second generation FRA1-AKT. Following initial model fitting, model refinement was performed by retaining only features with a variable importance projection (VIP) ≥ 1. The feature-reduced model was refit and displayed high quality with a strong fit ($R^2Y \approx 0.8$) and strong predictive performance ($Q^2Y \approx 0.75$). Given the few observations (**Y = 5**) used for model construction, permutations of the **Y** values were performed 500 times to generate null models and the performance of these was compared to the true model to evaluate the significance of model performance (Fig. 2C). The $pR^2Q = 0.03$ indicates that the model significantly outperformed null models.

The refined PLSR model identifies several features with positive coefficients for the prediction of peptide stability, including the C-terminal PEST score, instability index, and negative amino acid count following a shared CK2 consensus site (Fig. 3D). The proximity of the closest CK2 consensus site to the C-terminus is inversely associated with stability. Thus, increased distance of phospho-sites from the C-terminus is predicted to decrease protein stability. These features and patterns were considered for alterations designed to enhance stability in further experiments.

Feature	Feature Type	Feature Description
Term_pest_score	Physiochemical	The PEST score of the most C-terminal PEST domain.
pSite_prox_cterm	Positional	Distance of the most terminal CK2 consensus phosphorylation site ([S/T]-X-X-[D/E]) to the C-terminus.
AA length	Sequence	Length of regulatory protein segment that is fused to HSVtk.
CK2 consensus sites	Sequence	Number of occurrences of CK2 motifs ([S/T]-X-X-[D/E]) in the regulatory region.
pSite2_prox_cterm	Positional	Distance of the second most terminal CK2 consensus phosphorylation site ([S/T]-X-X-[D/E]) to the C-terminus.
Post_SPTE_instab	Physiochemical	Isoelectric point of C-terminal region following a shared CK2 motif present in all FRA1-based variants ("SPTE" sequence).
NegAAs_post_SPTE	Sequence	Number of negatively charged residues [E/D] in the C-terminus following shared CK2 motif.
PosAAs_post_SPTE	Sequence	Number of positive charged residues [H/L/R] in C-terminal region following shared CK2 motif.
Post_STPE_pI	Physiochemical	The isoelectric point (pI) of the C-terminal region following shared CK2 motif.

Table 1: Features descriptions from each FRA1-based regulatory region. Sequence, positional, and physiochemical features from each candidate regulatory region were gathered to use as predictive features for protein stability. The feature, feature type, and description are shown.

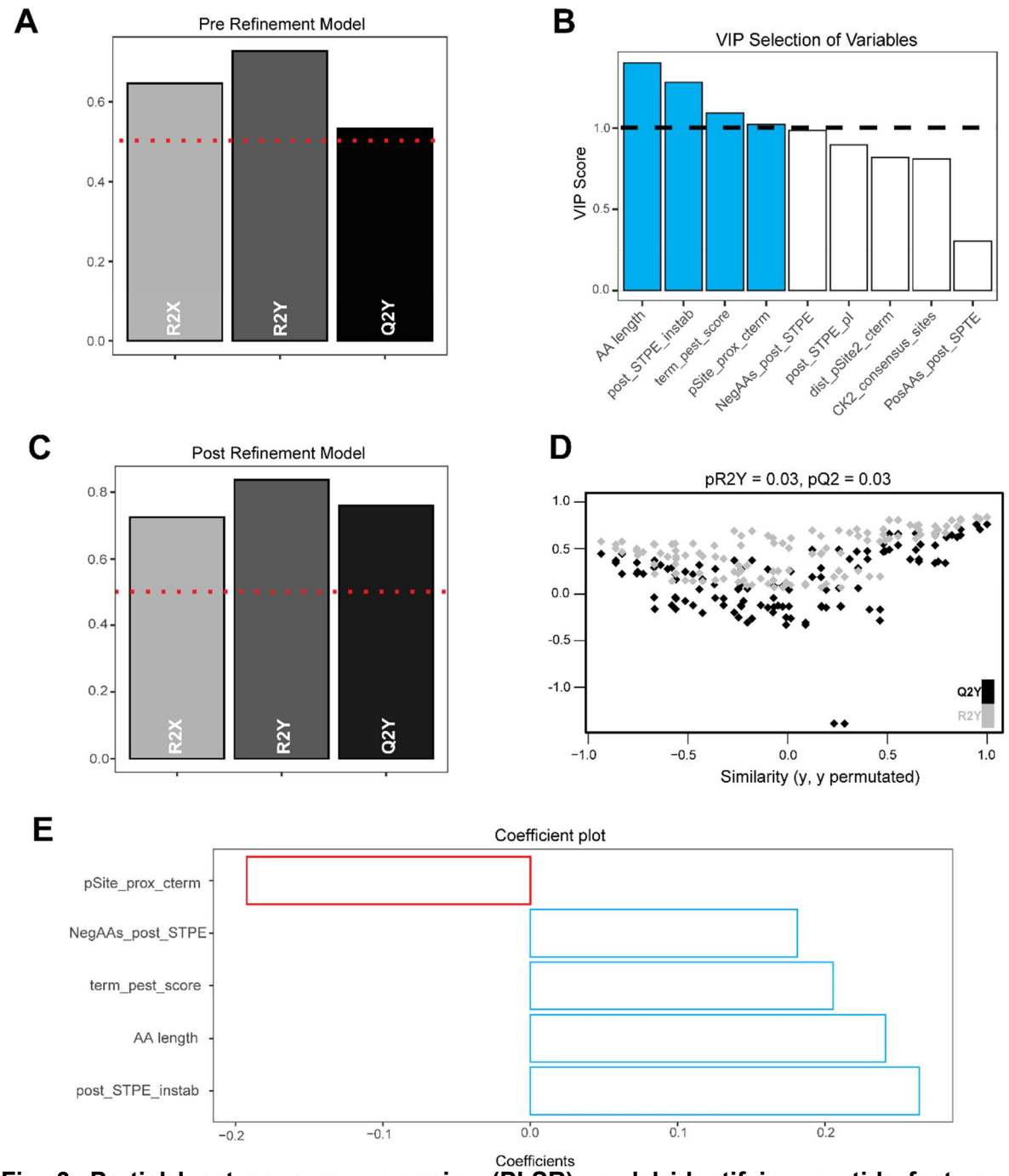

Fig. 3: Partial least squares regression (PLSR) model identifying peptide features that regulate stability. (A) Sequence, positional, and physiochemical features from each candidate regulatory region were gathered to use as predictive features for protein stability. An initial PLSR model was constructed based on characteristics of all FRA1-based regulatory proteins, the initial R^2X, R^2Y, and Q^2Y are shown. Dashed line indicates the typical threshold of 0.5 to indicate a model of good quality (B) VIP scores are shown for each feature in the initial PLSR model. (C) R^2X, R^2Y, and Q^2Y of the VIP-enriched PLSR model are shown. The model demonstrated strong predictive performance with an R^2X of 0.72, R^2Y of 0.84, and Q^2Y = 0.76. (D) Random permutation testing of y values to demonstrate model significance by comparing the actual model to null models. The probability of null model outperforming the actual model is quantified as pR^2Y of 0.03

and pQ^2 = 0.03. (E) Feature coefficients for the VIP-enriched PLSR model are shown. A positive coefficient indicates a feature predicted to contribute to peptide stability.

Engineering a second-generation FRA1-AKT peptide with enhanced stability

Insights derived from the PLSR model predicting protein stability were applied to develop a next-generation FRA1-AKT domain (FRA1-AKTgen2). Given the instability of the original FRA1-AKT variant, the next-generation integrated features predicted to enhance stability uncovered from the PLSR model. These adjustments included the addition of a more terminal CK2 consensus site to lessen instability and a compositional adjustment to enhance the terminal PEST score of FRA1-AKT (Fig. 4A). However, we were careful not to add extreme alterations here as these might affect CK2 sensitivity. This adjusted domain was then conjugated to HSVtk in a matching vector to the FRA1-AKT variant, and both were transduced in parallel to U87MG cells and sorted for GFP expression. For these, the GFP expression levels were not perfectly matched, so readings from these cells were normalized by their GFP co-expression. The baseline stability and CK2 sensitivity were measured first to examine whether alterations did increase stability and if CK2 sensitivity was retained. Transduced U87MG cells expressing AKT or AKTgen2 were treated with a CK2 inhibitor (CX-4945, 10 μM) or vehicle control (DMSO) and lysed following 48 hours of treatment. These lysates were immunoblotted, and the FLAG-tagged HSVtk fusion proteins were measured (Fig. 4B). It was apparent from the FLAG signal that the AKTgen2 fusion protein exhibited superior stability to AKT in the vehicle control samples and demonstrated a comparable reduction in signal when CK2 was inhibited (Fig. 4B). To further examine CK2 sensitivity, we examined the dose-dependent effect of CK2 inhibition (CX-4945, 10μM) using immunofluorescent staining and imaging for FLAG. Cells were treated for 48 hours, and the integrated intensity of FLAG was again normalized per cell by GFP co-expression due to expression differences (Fig. 4C). This experiment showed that the AKT and AKTgen2 variants exhibited a dose-dependent response to CK2 inhibition and reaffirmed that AKTgen2 demonstrated superior stability to AKTgen1 (Fig. 4C). These results indicate that

the small alterations in the peptide c-terminus vastly enhanced stability while CK2 sensitivity was retained (Fig. 3B, 3C).

Next, given that we wanted to enhance stability so that lower expression would still afford high cytotoxicity, we examined how each variant responded to treatment with the prodrug ganciclovir (GCV). Transduced U87MG cells expressing AKT and AKTgen2 were treated with GCV for 24 hours and fixed with paraformaldehyde. Immunofluorescent staining was then performed using the DNA-damage marker, γH2AX, as a readout for DNA damage, and the effect of GCV treatment was examined in a dose-dependent manner (Fig. 4C). GFP was also used to normalize γH2AX fluorescent intensity per cell to account for transcriptional differences. Here, it was apparent that the AKTgen2 variant was more sensitive to all concentrations of GCV, with a stark difference at higher doses (Fig. 4D). This suggests that the stability enhancements of AKTgen2 permitted enhanced DNA damage, presumably due to higher accumulation of HSVtk permitting more conversion of GCV into a cytotoxic product.

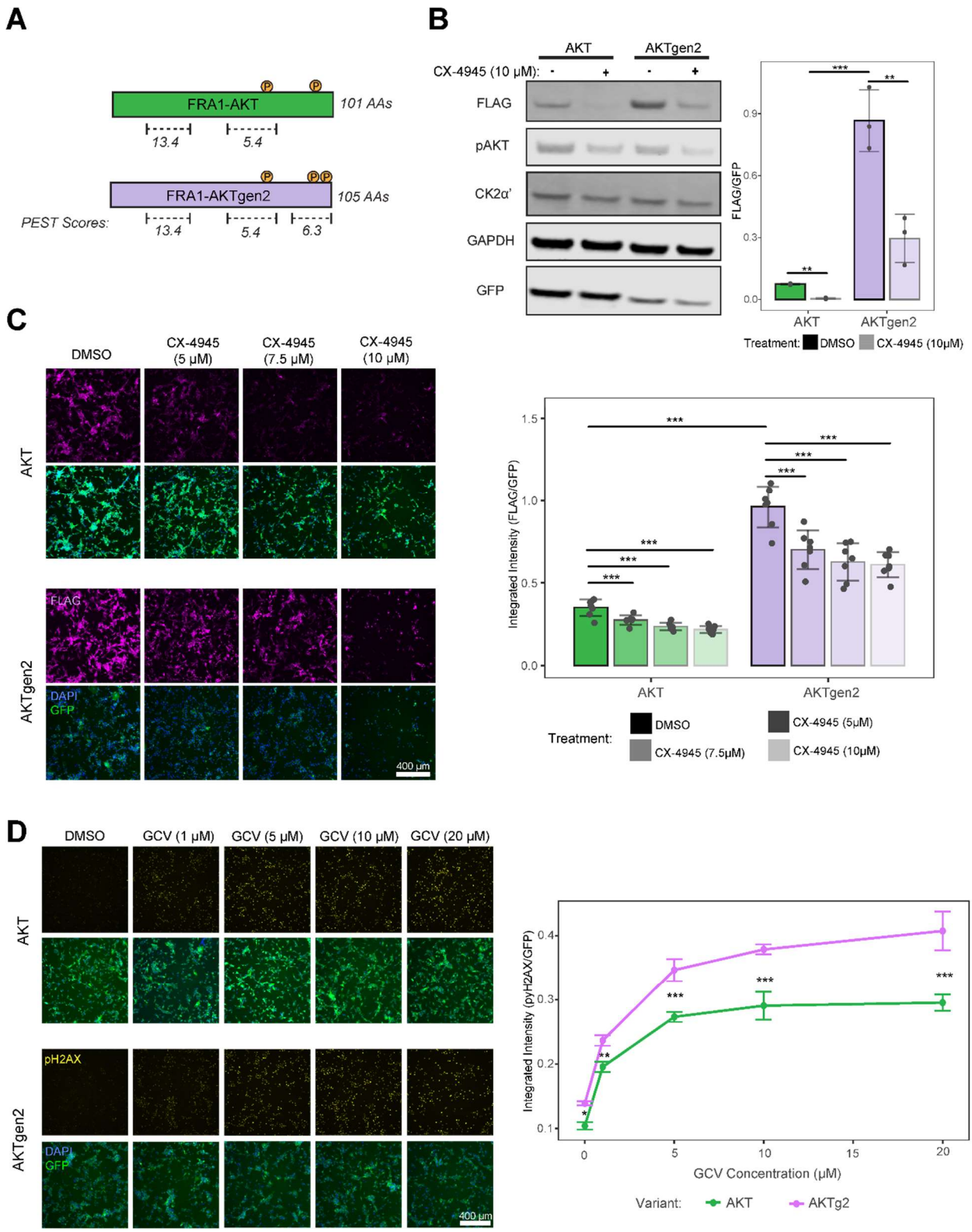

Fig 4: Design of second-generation fusion protein based on FRA1-AKT and evaluation of its properties. (A) The schematic shown highlights the differences between the AKT and AKTgen2 peptides, including the stronger terminal PEST-domain and additional CK2 phosphorylation site proximal to the C-terminus. (B) Flow-sorted U87MG cells expressing the

original FRA1-AKT or second-generation variant (FRA1-AKTgen2) were treated with CX-4945 (10 μM) or DMSO and lysed after 48 hr. Immunoblotting was performed using the indicated antibodies. Densitometry was used to quantify the GFP-normalized FLAG signal. Image is representative of n = 3 replicates, and data are plotted as mean ± sd. A two-way ANOVA and Tukey post-hoc test were applied to determine the significance of observed differences; *, **, and *** indicate p = 0.05, 0.01, or 0.001, respectively. (C) U87MG cells expressing the AKT-gen1 or -gen2 variants were treated with CX-4945 (5, 7.5, 10 μM) or DMSO for 48 hr. Immunofluorescence microscopy was performed using the indicated antibodies. Images are representative of n = 9 replicates, and data are plotted as mean ± sd. A two-way ANOVA and Tukey post hoc test were applied to determine the significance of observed differences; *, **, and *** indicate p = 0.05, 0.01, or 0.001, respectively. (D) Cells expressing AKT-gen1 or -gen2 were treated for 24 hr with 1- 20 μM GCV or DMSO and immunofluorescence microscopy was performed using the indicated antibodies. The GFP-normalized yH2AX was measured. Image is representative of n = 9 replicates, and data are plotted as mean ± sem. A two-way ANOVA with interaction and Tukey post hoc test were applied to determine the significance of observed differences; *, **, and *** indicate p = 0.05, 0.01, or 0.001, respectively.

Exploring the effect of subcellular localization on SGT sensitivity to CK2

To explore the effect of SGT fusion protein subcellular localization on regulation by CK2, we began by probing the localization of CK2α and CK2α' in U87MG cells using immunofluorescence microscopy. Quantification of nuclear-to-cytoplasmic FLAG revealed that both catalytic subunits are primarily nuclear, with the CK2α subunit starkly absent from the cytoplasm (Fig. 5A). Based on this distribution, we investigated the effect of SGT nuclear localization on cellular response to GCV by inserting an SV40 nuclear localization signal (NLS) before FLAG on the N-terminus of the SGT expression cassette (Fig. 5B). The NLS-containing cassette was inserted in pMSCV-IRES-GFP, and U87MG cells were transduced and flow-sorted to generate a population with similar GFP expression to transductants expressing the non-NLS version of the AKT-gen2 construct. Immunofluorescence microscopy revealed that the NLS version was completely nucleus-localized compared, whereas the non-NLS version was more evenly distributed within cells (Fig. 5C). Based on GFP-normalized FLAG expression, the NLS version was surprisingly relatively unresponsive to CK2 inhibition by CX-4945, while the cytoplasmic version demonstrated the anticipated reduction in FLAG expression (Fig. 5C). Baseline expression was unaffected by the addition of the NLS, contrary to what was previously

observed with the FRA1-based SGT[9]. The FRA1-AKTgen2 SGT lacking the NLS was used in the remainder of the experiments in this study.

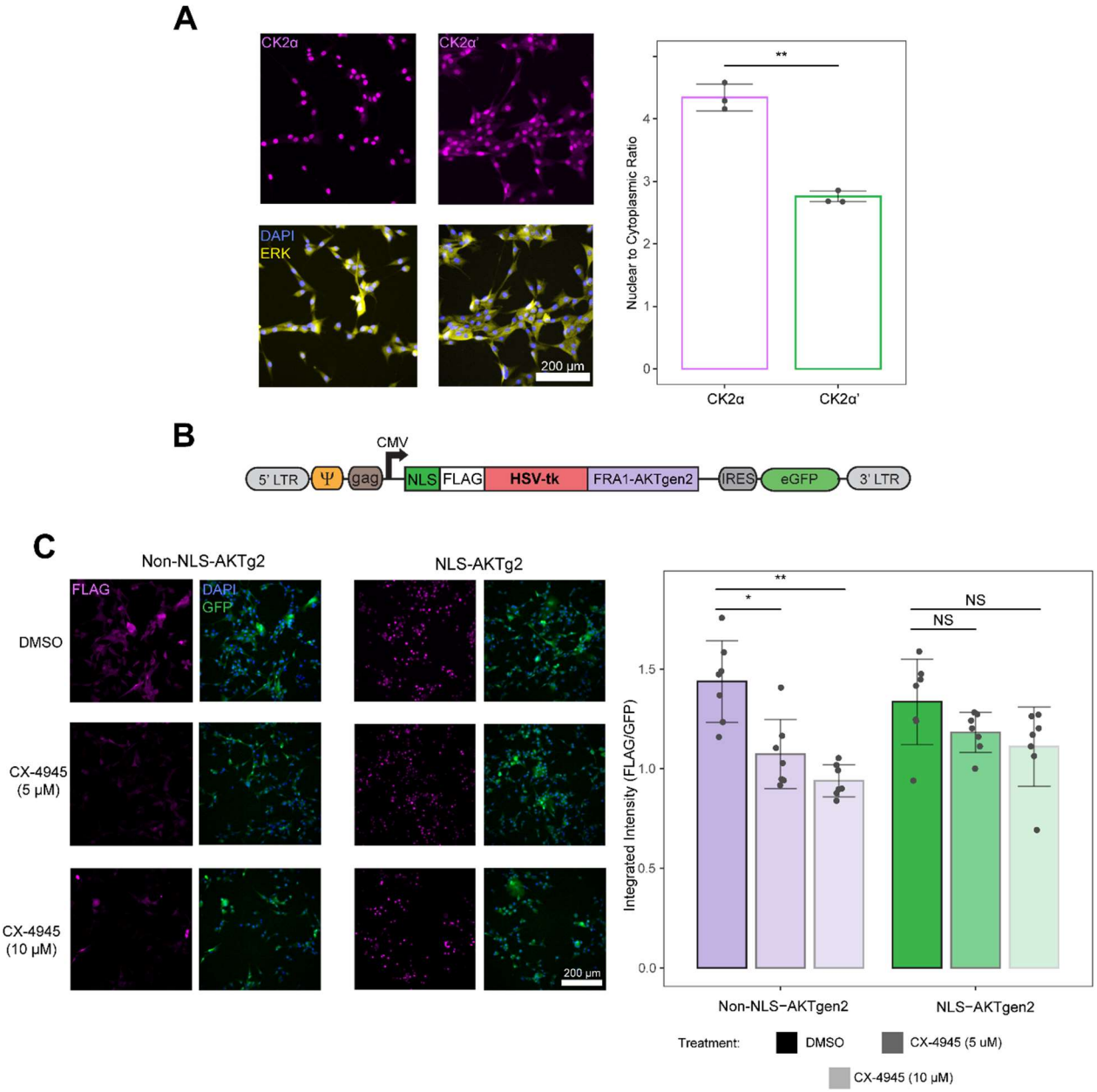

Fig. 5: Effect of fusion protein subcellular localization on regulation by CK2. (A) U87MG cells were subjected to immunofluorescence microscopy using antibodies against the two CK2 catalytic subunits. The nuclear-to-cytoplasmic ratio for both subunits was quantified as the average intensity in each. Mean values of nuclear to cytoplasmic ratios are reported. Image is representative of n = 3 replicates and data are plotted as mean ± sd. A Student's t test was applied to determine the significance of observed differences; *, **, and *** indicate p = 0.05, 0.01, or 0.001, respectively. (B) Schematic showing the design of a nucleus-localized version of the AKT-gen2 construct in which an SV40 NLS signal is inserted upstream of the FLAG-tagged HSVtk

fusion protein. (C) U87MG cells stably expressing the NLS and non-NLS versions of AKT-gen2 in an identical vector were flow-sorted to produce populations with similar GFP expression. Cells were then treated with CX-4945 at the indicated concentrations or with DMSO for 48 hr, and immunofluorescence microscopy was performed using antibodies against the indicated proteins. The expression of each variant was quantified as the GFP-normalized FLAG expression on a per-cell basis. Mean values to cytoplasmic ratios are reported. Image is representative of n = 6 replicates and data are plotted as mean ± sd. A two-way ANOVA with interaction and Tukey post hoc test were applied to determine the significance of observed differences; *, **, and *** indicate p = 0.05, 0.01, or 0.001, respectively.

Confirming specificity through shRNA targeting CK2

To confirm the CK2-specificity of regulation implied by studies using CX-4945 and to determine which of the CK2 subunits are responsible for SGT regulation, we engineered small hairpin RNAs (shRNAs) to generate a stable knockdown of CK2 α or α'. Two distinct, non-overlapping shRNAs were generated for each catalytic subunit plus a control shRNA that does not target any known human transcript. pLKO.1-puro lentiviral vectors encoding these shRNAs were used to transduce U87MG cells expressing AKTgen2. Based on immunoblotting of puromycin-selected transductants, CK2α was efficiently targeted by both hairpins, with one shRNA causing a potentially compensatory increase in CK2α' expression (Fig. 6A). FLAG expression was significantly reduced by both CK2α shRNAs. Only one CK2α' shRNA significantly decreased CK2α' and FLAG expression compared to the control (Fig. 6B). Interestingly, the relatively weak ~30% CK2α' knockdown achieved a reduction in SGT expression like that observed with a stronger CK2α knockdown, which may indicate stronger control of SGT expression by the CK2α’ subunit. To investigate the specificity of CK2 in driving SGT cytotoxicity, cells expressing control, CK2α, or CK2α' shRNAs were analyzed for response to GCV by flow cytometry. As expected, cell death in response to GCV was significantly decreased in cells expressing shRNAs against CK2α or CK2α' (Fig. 6C).

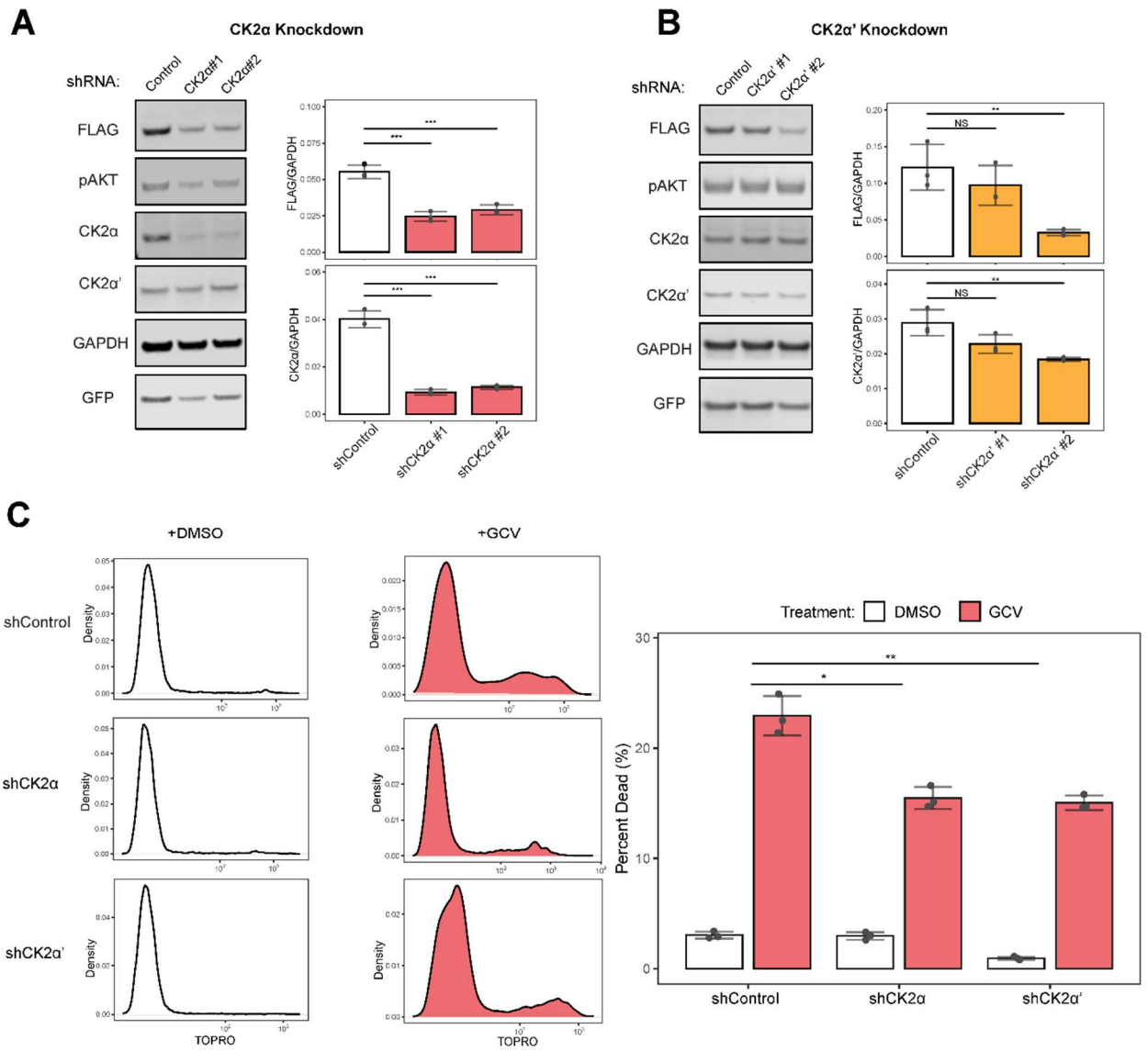

Fig. 6: Assessing the specificity of CK2 effects through stable knockdown of the catalytic subunits. (A,B) U87MG cells expressing AKT-gen2 were stably transduced with vectors encoding shRNA against CK2α or CK2α' or a control shRNA. Lysates were analyzed by immunoblotting using the indicated antibody. Densitometry was used to quantify the normalized FLAG signal. Image is representative of n = 3 replicates, and data are plotted as mean ± sd. A one-way ANOVA and Tukey post hoc test were applied to determine the significance of observed differences; *, **, and *** indicate p = 0.05, 0.01, or 0.001, respectively. (C) U87MG cells expressing AKT-gen2 and control shRNA or an shRNA targeting one of the CK2 catalytic subunits were treated for 3 days with 50 μM GCV or DMSO. Cell death was measured by flow cytometry. Cell distribution shown are representative of n = 3 replicates, and data are plotted as mean ± sd. A two-way ANOVA with interaction and Tukey post hoc test were applied to determine the significance of observed differences; *, **, and *** indicate p = 0.05, 0.01, or 0.001, respectively.

Investigating potential synergy between CK2-regulated SGT and chemotherapy

To determine if a CK2-regulated SGT would cooperate with chemotherapies used to treat glioblastoma, we measured the response of AKT-gen2 transductants to a combination of GCV with temozolomide (TMZ) or carboplatin. We hypothesized that a synergistic effect could occurs because CK2 contributes to DNA damage response and responds to stress signals; it seemed sensible that this could drive higher CK2 activity[26,27,29]. Carboplatin treatment resulted in a significant increase in FLAG expression compared to control, but TMZ had no effect (Fig. 7A). We also observed increased CK2α and CKα' expression with a stronger increase observed in carboplatin treated cells than TMZ (Supp. Fig. 1).

Given that. We further examined the extent of carboplatin-mediated effects on CK2 expression increase through immunofluorescence microscopy (Fig. 7B). AKT-gen2 transductants were plated in 96-well glass-bottomed plates for imaging and treated with a reduced carboplatin concentration (125 μM) to promote the retention of adherent cells. We found a significant enhancement in FLAG expression in response to carboplatin after 48 hr of drug treatment (Fig. 7B), confirming that carboplatin promotes the expression of the AKT-gen2 SGT.

Because we observed increased CK2α and CK2α' in carboplatin-treated cells (Fig. 6A, Supp. Fig. 1), we next examined if the carboplatin-dependent increase in AKT-gen2 expression relies on CK2 expression. In U87MG AKT-gen2 transductants expressing CK2 (α/α' catalytic subunits) or control shRNA, CK2α knockdown abrogated the carboplatin-mediated increase in SGT expression (Fig. 7C). Cells expressing a CK2α' shRNA (Fig. 7D) displayed a small but insignificant increase in SGT accumulation. In cells expressing the control shRNA, a significant increase in AKT-gen2 expression was observed in response to carboplatin, as expected. These results suggest a role for CK2 catalytic subunits in the enhancement of SGT expression and GCV-mediated cell death in AKT-gen2 transductants treated with carboplatin.

Finally, to determine quantitatively if carboplatin and GCV could exhibit synergy in driving cell death, U87MG AKTgen2 transductants were pre-treated with carboplatin or DMSO

for two days and then treated with GCV or a control treatment for three days. Carboplatin and GCV each independently induced reasonable levels of cytotoxicity (~15% or ~35% reduction in cell viability, respectively), as determined by flow cytometry. When GCV and carboplatin were combined, however, a more than 90% reduction in cell viability was observed (Fig. 7E), indicating a strong synergistic effect. To quantify the degree of synergy, we used an effect-based Bliss Independence model[71]. According to the Bliss model, the combination index (CI) is computed as $CI = \left(E_A + E_B - E_A E_B\right) / E_{AB}$, where E_A and E_B are the effects (ex. Loss in viability) of individual treatments and E_{AB} is the effect of the combination treatment[71]. CI < 1 indicates synergy, and CI > 1 indicates antagonism. Using the percent of dead cells as the effect, CI ≈ 0.3 for the combination of GCV and carboplatin indicates a high degree of synergy.

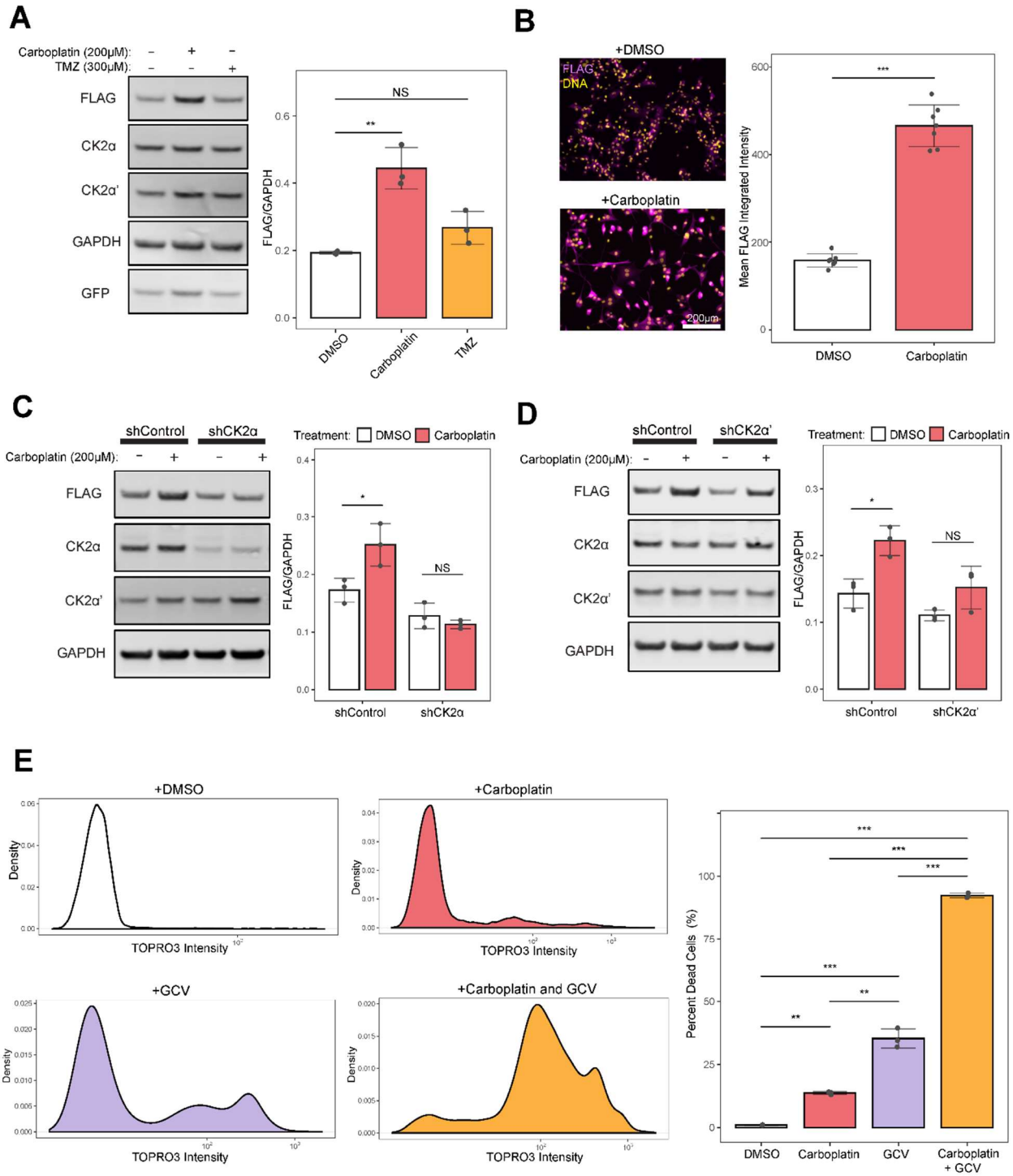

Fig. 7: Evaluating potential synergies between CK2-regulated SGT and chemotherapy. (A) U87MG cells expressing AKT-gen2 were treated with carboplatin (200 μM), TMZ (300 μM), or DMSO and lysed after 48 hr. Immunoblotting was performed using the indicated antibodies. Densitometry was used to quantify the GAPDH-normalized FLAG signal. Image is representative of n = 3 replicates, and data are plotted as mean ± sd. A one-way ANOVA and post hoc Tukey test were applied to determine the significance of the indicated differences; *, **, and *** indicate p = 0.05, 0.01, or 0.001, respectively. (B) Cells were treated with carboplatin (125 μM) or DMSO

for 48 hr and immunofluorescence microscopy was performed using antibodies against the indicated proteins. The expression of each variant was quantified as the mean FLAG expression on a per-cell basis. Image is representative of n = 6 replicates and is plotted as mean ± sd. A Student's t test was applied to determine the significance of the indicated differences; *, **, and *** indicate p = 0.05, 0.01, or 0.001, respectively. (C, D) Cells expressing AKT-gen2 and a control shRNA or an shRNA targeting CK2α (C) or CK2α' (D) were treated with carboplatin (200 μM) or DMSO for 48 hr and lysed. Immunoblotting was performed using the indicated antibodies. Densitometry was used to quantify the GAPDH-normalized FLAG signal. Images are representative of n = 3 replicates, and data are plotted as mean ± sd. A Student's t test was applied within each shRNA group to determine the significance of the indicated differences; *, **, and *** indicate p = 0.05, 0.01, or 0.001, respectively. (E) Cells expressing AKT-gen2 were pre-treated with DMSO or carboplatin (200 μM) for two days, followed by treatment with DMSO or GCV (50 μM) administration for three days. Cell death was then measured by flow cytometry through TOPRO staining. Data displayed is representative of n = 3 replicates and data are plotted as mean ± sd. A one-way ANOVA and post hoc Tukey test were applied to determine the significance of the indicated differences; *, **, and *** indicate p = 0.05, 0.01, or 0.001, respectively.

2.5 DISCUSSION

In this study, we engineered a novel suicide gene therapy that is post-translationally regulated by CK2 activity. This SGT conceptual design builds on a previously constructed ERK-regulated SGT, which leveraged overactive signaling to target cancer cells selectively[9]. However, a notable advancement of the CK2-regulated SGT was engineering a non-native interaction with CK2 using the FRA1 sequence as a scaffold. This CK2-regulated SGT is also distinct from the few other examples of post-translationally regulated SGTs that used a fragment of a natural substrate for regulation via hypoxia response[72]. We demonstrated the CK2 specificity of our SGT through inhibitor and knockdown studies, revealing dynamic changes in accumulation concurrent with alterations in CK2 activity. We also demonstrated the potential ways this SGT could be used as a combination treatment with chemotherapy, which exhibited high synergy with carboplatin (Fig. 7). While we demonstrated specific regulation by CK2, we did not observe full loss of SGT accumulation despite CK2 inhibition (Fig. 4) or knockdown (Fig. 6). Overall, our approach to engineering non-native interactions for SGT regulation

demonstrates a potentially powerful tool that could be expanded to other kinases or possibly leveraging other post-translational modifications for regulation.

Our initial screen of candidate peptides revealed one responsive variant that was also the least stable. Previous issues in SGT attempts have highlighted a shortcoming is insufficient conversion of prodrugs to toxic metabolites, which can be drive by low expression or protein stability[8]. Since we achieved high expression through a CMV promoter, we aimed to enhance the SGT protein stability while not disrupting CK2 sensitivity. Optimally, we would have built accurate structural models to uncover important features of the FRA1 PEST backbone that permit enhanced phosphorylation-based stabilization, but insight into the structure is limited due to low confidence predictions of the PEST domain present the C-terminus of FRA1[42]. Additionally, advanced models such as AlphaFold[42] are not capable of predicting the structural effect of post-translational modifications[73]. While massive leaps in structural biology have allowed for the accurate prediction of protein structures from sequences alone, these techniques perform poorly on disordered protein regions where PEST motifs are often located[43,44]. This led us to select a simpler machine learning model (PLSR) to predict stability and mine sequence-based features using all our candidate peptides, which displayed higher stability. (Fig. 2 & 3, Supp. Table 1). Our model helped us resolve key features that predicted stability that we were able to implement into our following SGT design. These alterations did indeed enhance stability and drive increased DNA damage (Fig. 4).

The FRA1 PEST domain demonstrates the remarkable property of phosphorylation-based stabilization; this led us to its sequence as a scaffold to build most of our peptides. This region appears to be specialized in endogenous FRA1 and its relative FOS, which share high conservation in the C-terminus; both demonstrate switch-like stabilization when phosphorylated in their C-terminal PEST domains[74,75]. Mechanisms for how this alteration stabilizes these proteins are unknown, but it has been demonstrated that the terminal PEST domain of FOS undergoes a conformational change when phosphorylated by ERK. This was facilitated by

disruption of interactions between the phosphorylated serine and its proline neighbor located immediately downstream (n+1), leading to destabilization of a turn structure near the C-terminus[76]. Notably, this terminal ERK phosphorylation site shares the same sequence (“SPTL”) as FRA1 proximal to residues promoting a helical structure[77]. We found that the only responsive variants in this study incorporated a relatively similar terminal phosphorylation site conforming to the minimal CK2 consensus sequence ([S/T]-X-X-[D/E] with a proline at the n+1 position (“SPSD”). Additionally, there is evidence of phosphorylation-mediated alterations in local structure in other intrinsically unstable proteins. For example, the sodium proton exchanger 1 (NHE1) contains two terminal phosphorylation sites targeted by MAPK1 that, upon phosphorylation, stabilize transient helices[78]. Here it was found that a helix stabilization motif conforming to sequence “[S/T]-P-XXX-[R/K]” was well-represented surrounding phosphorylation sites throughout the proteome[78]. Notably, this phosphorylation-tunable helix, like FRA1, FOS, and the CK2-regulated SGT, contain a terminal phospho-site with proline at the n+1 position. It is possible that this interaction between serine and proline contributes to the phosphorylation-induced stabilization effect in FRA1 and FOS; however, we are uncertain whether this interaction is conserved in the CK2-regulated SGT. Further work using site-directed mutagenesis of the CK2-regulated SGT could confirm that the “SPSD” sequence conveys phosphorylation induced stability. If indeed responsible, investigating the structural alterations mediated by phosphorylation of these residues with circular dichroism spectroscopy could inform how local protein structures are altered and how these properties could be further improved.

Of particular interest for translational applications was our investigations combining SGTs with chemotherapies. This work revealed synergy between carboplatin and the CK2-regulated SGT (Fig. 7). Pre-treatment of cells expressing the SGT with carboplatin followed by GCV led to significant enhancements in cytotoxicity compared to treatment with either carboplatin or GCV alone. The role of CK2 in resistance to platinum-based drugs (carboplatin,

cisplatin) could indicate why this combination was effective. CK2 drives resistance to this drug class by driving increased DNA damage repair through MDC1 and XRCC1[29]. It has also been shown that CK2 inhibition reverses cisplatin resistance in lung adenocarcinoma and gastric cancer models[79], and CK2 combined with cisplatin is actively being tested in clinical trials for cholangiocarcinoma, highlighting the potential for CK2 in response to platinum-based drugs (NCT02128282). CK2 expression has also been shown to increase in response to cisplatin in lung cancer cells[80]; in this study, we did observe an increase in CK2α and α' accumulation when treated with carboplatin (Fig. 7A, Supp Fig. 1). Carboplatin-induced overexpression or decreased CK2 turnover would be a sensible explanation for our observed increases in SGT levels (Fig. 7A) that were abrogated when CK2 expression was knocked down. While much is unknown about the mechanisms of upregulated CK2 expression, STAT3 has previously been shown to be enriched in CK2 promoters and induce higher CK2α expression in PTEN knockout cells[81]. In addition, platinum-based drugs have been shown to drive STAT3 activation and transcription of genes related to DNA damage repair[82]. This mechanism could explain our observations of increased CK2α/α' U87MG cells, which express a hypomorph of PTEN[83,84]. In further investigation, it would also be interesting to evaluate whether cells with normal PTEN increase CK2 expression in response to platinum-based and if these chemotherapies.

We were surprised that TMZ, another DNA-damaging chemotherapy, did not induce increased CK2-SGT accumulation. Following treatment with TMZ, we observed a small but insignificant increase in SGT accumulation (Fig. 7A). We also observed that CK2α' increased with TMZ treatment, although to a lower degree than carboplatin treated cells (Supp Fig. 1). If STAT3 is responsible for driving increased CK2 following carboplatin treatment, it is likely that this mechanism would be observed in TMZ treated cells. STAT3 is overactive in cells cultured with TMZ to generate treatment resistance[85]. Due to this, we expect that longer treatments or higher doses of TMZ might elicit a similar response in SGT accumulation and CK2 expression.

We were also surprised to uncover that a nuclear localized version of the SGT was less sensitive to CK2 inhibition. When optimizing our most promising SGT, we found that both CK2α and CK2α' displayed high nuclear localization (Fig. 5A). We expected that increasing the colocalization of the SGT with CK2 catalytic subunits would enhance their sensitivity to CK2 activity. However, we observed the opposite relationship with the cytoplasmic SGT exhibiting higher sensitivity to CK2 inhibition (Fig. 5C). It is possible that this could be explained by the localization of CK2β, which we did not study in this work. Association between the catalytic subunits (α/α') and regulatory subunits (β), as well as subcellular localization, can alter substrate specificity[20,86,87]. The formation of a tetramer composed of α and β subunits can completely prevent interaction with some substrates and it has previously been shown that CK2β is also primarily nuclear localized[88]. It is possible that a high colocalization of all subunits in the nucleus favors holoenzyme formation, which might reduce affinity for the CK2-regulated SGT. An alternative perspective arises from CK2 preference for AKT family proteins, where AKT1, which is targeted by CK2, is predominantly cytoplasmic and AKT2 is nuclear[89]. Intriguingly, CK2 avoids phosphorylating AKT2 despite a high sequence consensus with AKT1[90]. Our top SGT candidates, AKT and AKT-gen2, utilized an AKT1 segment to attract CK2 phosphorylation. Hence, it is plausible that the specific SGT sequence was more readily targeted by CK2 in the cytoplasm. Lastly, the reduced sensitivity of the nuclear SGT could also be a consequence of the inhibitor, which might not penetrate the nucleus as effectively. In further work, additional knockdowns of all subunits should be performed and examination of whether our SGT is β-independent or -dependent substrate should be examined.

Suicide gene therapies provide an alternate approach to cancer therapy by leveraging cancer-intrinsic properties to induce selective cytotoxicity. Despite the promise of SGTs, they have thus far failed to provide clinical benefit. Key criteria for the success of these therapies are cancer specificity and sufficient expression. In this work, we describe an SGT that meets both criteria, achieving specificity through engineering a post-translational stability switch regulated

by CK2 and high expression through a strong viral promoter (CMV). Furthermore, our work illustrates the potential application of a CK2-regulated SGT in combination with carboplatin to heighten therapeutic efficacy.

2.7 SUPPLEMENTARY MATERIALS

FRA1-CK2	LVLEAHRPICKIPEGAKEGDTGSTSGTSSPPAPCRPVPCISLSPGPVLEPEALHTPTLMTTPSLTPFTPSLV**S**TPEPCASAHR EE**S**EDEEDPEDDPEE**S**P**T**EDEELLAL
FRA1-CK2.2	LVLEAHRPICKIPEGAKEGDTGSTSGTSSPPAPCRPVPCISLSPGPVLEPEALHTPTLMTTPSLTPFTPSLV**S**TPEPCASAHR KESS**S**S**S**EDES**S**DPEESPE**S**P**T**EDEELLAL
FRA1-AKT	LVLEAHRPICKIPEGAKEGDTGSTSGTSSPPAPCRPVPCISLSPGPVLEPEALHTPTLMTTPSLTPFTPSLV**S**TPEPCASAHR K**S**PSDNAGAEEMPTLLAL
FRA1-CAM	LVLEAHRPICKIPEGAKEEDEGSTSGTP**S**DPEEDRPVPCISLSPGPVLEPEALHPEDEEDSP**S**LEEDDPSED**S**TPEPEEDA HDDE**S**DDDWDDDLDDD**S**DDDWAL
FRA1-stCK2	LVLEAHRPICKIPEGAKEGEPSPDPEEPEPEEDERPVPCISLSPGPVLEPEALHTPTLMTTPSLTPFTPSLV**S**TPEPCASAHR EE**S**EDEEDPEDDPEE**S**P**T**EDEELLAL
NOVEL PEST	KKGSLLRVSAMFVKEGEPDPDEE**S**EEDEEPEPEEDEPEEGEEKVAMSFESFVKEDEE**S**DEDEPPDEDDEDDEDESDKVA SMFSLLR
FRA1-AKTgen2	LVLEAHRPICKIPEGAKEGDTGSTSGTSSPPAPCRPVPCISLSPGPVLEPEALHTPTLMTTPSLTPFTPSLV**S**TPEPCASAHR K**S**PSDNAGAEE**S**PSDPTLLAL

Supplementary Table 1: Sequences of candidate regulatory regions. Amino acid composition of all regulatory region variants. CK2 consensus phosphorylation sites conforming to a [S/T]-X-X-[D/E] pattern are underlined and predicted phosphorylated residues are shown in bold. Areas highlighted in are PEST regions with scores > 5 using the EMBOSS epestfind[68] webtool.

CK2 Sites/Scores	FRA1-CK2	FRA1-CK2.2	FRA1-AKT	FRA1-CAM	FRA1-stCK2	Novel PEST	FRA1-AKTgen2
Site 1 Sequence	**S**PTE	**S**PTE	**S**PTE	**S**DPE	**S**TPE	**S**EED	**S**PTE
Site 1 (CK2α)	74.1	74.1	74.1	98.1	74.1	99.5	74.1
Site 1 (CK2α')	77.5	77.5	77.5	97.9	77.5	99.8	77.5
Site 2 Sequence	**S**EDE	**S**SSE	**S**PSD	**S**LEE	**S**EDE	**S**DED	**S**PSD
Site 2 (CK2α)	99.7	91.1	63.6	95.3	99.7	99.9	63.6
Site 2 (CK2α')	99.8	90.5	65.4	94.9	99.8	99.9	65.4
Site 3 Sequence	**S**PTE	**S**EDE	NA	**S**TPE	**S**PTE	NA	**S**PSD
Site 3 (CK2α)	96.3	97.7	NA	91.3	96.3	NA	63.6
Site 3 (CK2α')	96.9	97.8	NA	93.4	96.9	NA	65.4
Site 4 Sequence	**T**EDE	**S**DPE	NA	**S**DDD	**T**EDE	NA	NA
Site 4 (CK2α)	98.3	99.6	NA	99.8	98.3	NA	NA
Site 4 (CK2α')	98.5	99.7	NA	99.9	98.5	NA	NA
Site 5 Sequence	NA	**S**PTE	NA	**S**DDD	NA	NA	NA
Site 5 (CK2α)	NA	94.7	NA	99.9	NA	NA	NA
Site 5 (CK2α')	NA	95.5	NA	99.9	NA	NA	NA
Site 6 Sequence	NA	**T**EDE	NA	NA	NA	NA	NA
Site 6 (CK2α)	NA	97.8	NA	NA	NA	NA	NA
Site 6 (CKα')	NA	97.9	NA	NA	NA	NA	NA

Supplementary Table 2: **CK2 consensus sites and affinities for regulatory substrates**. Each consensus site underlined in Supp. Table 1 was scored using the KinaseLibrary tool[51] for affinity to CK2α and CK2α'. The first residue, shown in bold, of each consesus site represents the residue that could be phosphorylated.

FEATURES	FRA1_CK2	FRA1_CK2.2	FRA1_AKT	FRA1_CAM	ST_FRA1_CK2
pSite_prox_cterm	8	8	16	6	8
AA length	109	110	101	105	109
term_pest_score[1]	29.44	25.9	-4.69	0	29.44
pSite2_prox_cterm	28	10	28	19	10
CK2_consensus_sites	4	5	2	5	4
NegAAs_post_STPE[2]	17	12	4	20	17
PosAAs_post_SPTE[2]	1	2	2	0	1
post_STPE_aliphatic[2]	39.73	38.68	57.59	29.7	39.73
post_STPE_pI[3]	3.54	3.91	4.83	3.1	3.54

Supplementary Table 3: Protein features predictor set (X) for PLSR model. The pSite (pSite_prox_cterm, pSite2_prox_cterm) and PEST (pos_PEST_dist_cterm) proximity features were calculated as the distance between the peptide C-terminus and the mentioned feature. Phosphorylation site (pSite) terms were determined by sequences conforming to the CK2 minimum consensus sequence ([S/T]-X-X-[E/D]. Features annotated "post_STPE" were calculated after aligning sequences displaying a short consensus sequence (SPTE) that was shared between all FRA1-based variants. Features describing PEST scores (term_pest_score, avg_pest) were obtained through the ePestfind webtool[68]. The instability index, isoelectric points (pI), positive amino acids (PosAAs), and negative amino acids (NegAAs) features were collected using the Expasy ProtParam webtool[67].

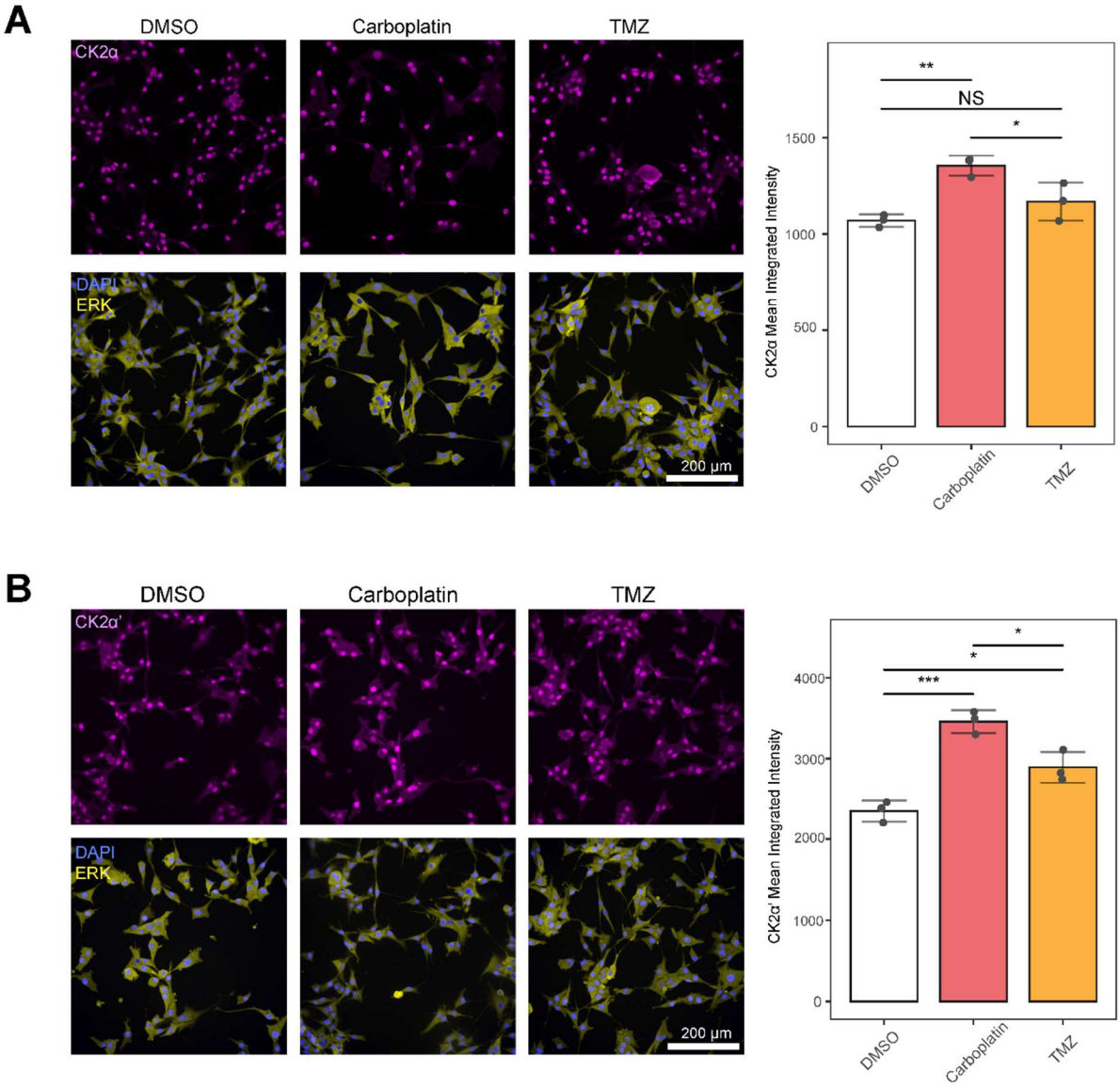

Supplementary Figure 1: Effect of TMZ or carboplatin on CK2 expression. U87MG cells were subjected to immunofluorescence microscopy using antibodies against the two CK2 catalytic (A: CK2α, B: CK2α') subunits. Image is representative of n = 3 replicates and data are plotted as mean ± sd. A Student's t test was applied to determine the significance of observed differences; *, **, and *** indicate p = 0.05, 0.01, or 0.001, respectively.

CHAPTER 3: CONCLUSIONS AND FUTURE WORK

3.1 SUMMARY

The work in this thesis describes the development, optimization, and validation of a SGT post-translationally regulated by CK2 signaling. This system leverages the overactive CK2 signaling frequently observed in many cancers, notably glioblastoma, to stabilize an unstable peptide fused to HSVtk through phosphorylation. To develop this technology, we investigated CK2 substrates, designed a panel of candidate peptides incorporating CK2 target sites fused to HSVtk, and discovered one candidate demonstrating responsiveness (i.e., increased turnover) to CK2 inhibition. Further, we utilized measurements and computed features from the whole peptide panel to build a partial least squares regression model to uncover the peptide characteristics that promote stability. Using insights from this model, we built a second version of the CK2-regulated peptide that demonstrates improved stability. Further, we investigated the effect of subcellular localization on the candidate SGT's sensitivity to CK2 activity, demonstrated specific regulation of the novel SGT by CK2 through knockdown experiments of CK2 catalytic subunits, and uncovered an ability for the CK2-regulated SGT and the chemotherapeutic agent carboplatin to synergistically kill GBM cells.

In addition to creating a novel CK2-regulated suicide gene therapy vector, this work highlights the potential for post-translationally regulated gene therapies. Our lab previously developed a similar suicide gene vector that relies on the kinase ERK to stabilize a PEST domain from FRA1[9]. This prior work utilized an endogenous target domain that is natively phosphorylated and stabilized by ERK, which was previously applied as a live-cell reporter[60]. While heavily inspired by the ERK-regulated SGT, the work detailed here illustrates a novel approach where a *de novo* protein was engineered to be targeted by CK2 and subsequently stabilized by phosphorylation. The most promising CK2-regulated SGTs described were based on a FRA1 PEST backbone, which is not known to be targeted by CK2. However, it also

demonstrates that inherent features of the FRA1 PEST domain can serve as a platform for developing phospho-stabilized proteins targeted by alternative kinases for either new therapies or activity reporters.

A challenge In this project was the lack of understanding and consensus regarding mechanisms regulating CK2. In our previous work with ERK, it was relatively straightforward to alter ERK activity as the mechanisms governing its activation are well-known and tightly regulated. However, CK2 acts as a constitutively active kinase, with catalytic subunits maintaining activity alone or while engaged with a regulatory subunit. In addition, the mechanisms regulating CK2 activity and expression are poorly understood[20]. This lack of understanding regarding CK2 regulation made it more challenging to induce increased CK2 activity; however, we achieved lower activity through inhibitor and knockdown of catalytic CK2 subunits. These experiments demonstrated that our SGT was specifically regulated by CK2 activity, but we did not investigate the role of the regulatory subunit CK2β. It has previously been found that some substrates can only be phosphorylated by CK2 when associated with CK2β or that their propensity for targeting is substantially enhanced in the presence of CK2β [20,24,87]. Further investigations on the role of CK2β through knockdown studies could be interesting to understand how the SGT described here is targeted.

One of this study's most exciting and promising results was the interaction between the final CK2-regulated SGT and carboplatin. We found that treatment of GBM cells with carboplatin induced significantly higher expression of the AKT-gen2 SGT. Knockdown experiments demonstrated that the enhancement in SGT expression depends on CK2. We also found that pre-treatment with carboplatin, followed by prodrug administration, led to an even more substantial cytotoxic effect. Further, the Bliss Independence model[71] for effect-based quantification indicated that the combination of carboplatin and GCV is highly synergistic at inducing cell death. Since carboplatin and TMZ are DNA-damaging agents, it was somewhat surprising that TMZ did not induce higher SGT accumulation. However, we expect that this

difference might be due to the degree of DNA damage induced by each drug at the tested concentrations or time. We noticed enhancements in CK2 expression following carboplatin and TMZ treatment but to a lesser extent in TMZ treated cells. Further testing with higher doses or longer incubation with TMZ is warranted to induce higher DNA damage, which might further increase CK2 expression and subsequent SGT accumulation. CK2 is known to be heavily involved in multiple DNA damage response pathways[28,29] so we would expect that other chemotherapies or radiotherapy might also synergize with the CK2-regulated SGT and warrant further investigation.

3.2 FUTURE DIRECTIONS

Extension to other cell lines and animal models

The reliance of this work on the U87MG cell line limits insights into the therapeutic potential. U87MG cells have been a staple cell line for GBM research and the most common cell line applied for its study, but they fail to recapitulate some behaviors of GBM cells and represent only one genetic background[91]. For example, in mouse tumor xenograft studies, U87MG cells form large, homogenous, and well-vascularized tumors with clean borders[92]. These characteristics are largely absent from real GBM tumors, which limits the translation of the cell line models we engineered for *in vivo* studies.

Exploring alternative cellular contexts, particularly glioma-initiating cells (GICs), offers the potential to capture the dynamic nature of glioblastoma multiforme (GBM) more accurately. When orthotopically implanted, these cells can faithfully reproduce the intratumoral heterogeneity and invasiveness characteristic of GBM[92]. Of particular note is the pivotal role played by GICs in driving chemoresistance within glioblastoma tumors[92]. In light of this, GICs represent an ideal choice for in vivo studies involving the novel SGT we have engineered. Our experimental procedures thus far have been confined to a two-dimensional setting on tissue

culture plastic. This approach fails to fully encapsulate the intricate complexities of the tumor microenvironment, thereby limiting our ability to assess comprehensively how viral delivery of SGT influences efficacy.

Additionally, moving to an *in vivo* setting would allow exploration of how the therapy impacts noncancerous cells and allow for an assessment of the magnitude of bystander toxicity in untransduced cells. This evolution to an *in vivo* paradigm would not only advance the translational potential of our research findings but also ensure a more comprehensive evaluation of the therapeutic intervention within a physiologically meaningful context.

Uncovering mechanisms regulating proteasomal degradation of SGTs

The FRA1 PEST domain was used as a backbone for engineering CK2-regulated SGTs, largely due to its instability and known phosphorylation-dependent stabilization. An interesting feature of FRA1 and its relative FOS is their capability to undergo ubiquitin-independent or -dependent proteasomal degradation[61,77,93]. ERK phosphorylation in C-terminal PEST domains of both FOS and FRA1 prevents ubiquitin-independent proteasomal degradation[61,77]. This degradation mechanism appears critical for ERK-mediation stabilization and, as a result, the ERK-regulated SGT[9]. However, we do not know if this mechanism is conserved in the CK2-regulated SGT. It is conceivable that the mechanism would be maintained due to the use of a FRA1 PEST backbone, but previous studies have also demonstrated that phosphorylation of PEST domains can also lead to ubiquitin-dependent targeting[94]. PEST domains have been thought to be degraded by default by the ubiquitin-independent proteasomal degradation[94], which would serve as an advantage for these SGT systems to ensure quick turnover, allowing more dynamic regulation. Further studies investigating more granular time-dependent changes in SGT accumulation, mutagenesis of lysine residues, and probing for the presence of ubiquitination could allow us to understand how this SGT is processed.

Exploring synergistic effects of CK2-regulated SGT with radiotherapy and diverse chemotherapeutic agents

In our current investigation, we successfully established the potent synergy between CK2-regulated SGT and carboplatin treatment. However, our exploration was limited to the interaction of the SGT with only two conventional chemotherapeutic agents, and we observed no discernible response with TMZ at the tested dose and duration. We posit that further investigation into TMZ may unveil a comparable effect, considering CK2's pivotal role in DNA damage repair and evasion of apoptosis[26,28,29]. Previous studies have consistently demonstrated the synergistic outcomes of combining CK2 inhibition with various chemotherapy drugs[33,34], emphasizing the potential for further enhancement through the integration of CK2-regulated SGT. This underscores the necessity for testing additional DNA damaging drugs to unveil and capitalize on the full spectrum of synergistic effects with CK2-SGT.

REFERENCES:

1. Hossain, J.A., Marchini, A., Fehse, B., Bjerkvig, R., and Miletic, H. (2020). Suicide gene therapy for the treatment of high-grade glioma: past lessons, present trends, and future prospects. Neurooncol Adv *2*, vdaa013. 10.1093/noajnl/vdaa013.
2. Zarogoulidis, P., Darwiche, K., Sakkas, A., Yarmus, L., Huang, H., Li, Q., Freitag, L., Zarogoulidis, K., and Malecki, M. (2013). Suicide Gene Therapy for Cancer - Current Strategies. J Genet Syndr Gene Ther *4*. 10.4172/2157-7412.1000139.
3. Bulcha, J.T., Wang, Y., Ma, H., Tai, P.W.L., and Gao, G. (2021). Viral vector platforms within the gene therapy landscape. Signal Transduct Target Ther *6*, 53. 10.1038/s41392-021-00487-6.
4. Tamura, R., Miyoshi, H., Yoshida, K., Okano, H., and Toda, M. (2021). Recent progress in the research of suicide gene therapy for malignant glioma. Neurosurg Rev *44*, 29-49. 10.1007/s10143-019-01203-3.
5. Pandha, H.S., Martin, L.A., Rigg, A., Hurst, H.C., Stamp, G.W., Sikora, K., and Lemoine, N.R. (1999). Genetic prodrug activation therapy for breast cancer: A phase I clinical trial of erbB-2-directed suicide gene expression. J Clin Oncol *17*, 2180-2189. 10.1200/JCO.1999.17.7.2180.
6. Fujiwara, T., Urata, Y., and Tanaka, N. (2007). Telomerase-specific oncolytic virotherapy for human cancer with the hTERT promoter. Curr Cancer Drug Targets *7*, 191-201. 10.2174/156800907780058835.
7. Shirakawa, Y., Tazawa, H., Tanabe, S., Kanaya, N., Noma, K., Koujima, T., Kashima, H., Kato, T., Kuroda, S., Kikuchi, S., et al. (2021). Phase I dose-escalation study of endoscopic intratumoral injection of OBP-301 (Telomelysin) with radiotherapy in oesophageal cancer patients unfit for standard treatments. Eur J Cancer *153*, 98-108. 10.1016/j.ejca.2021.04.043.
8. Karjoo, Z., Chen, X., and Hatefi, A. (2016). Progress and problems with the use of suicide genes for targeted cancer therapy. Adv Drug Deliv Rev *99*, 113-128. 10.1016/j.addr.2015.05.009.
9. Day, E.K., Campbell, A., Pandolf, A., Rogerson, T., Zhong, Q., Xiao, A., Purow, B., and Lazzara, M.J. (2021). ERK-dependent suicide gene therapy for selective targeting of RTK/RAS-driven cancers. Mol Ther *29*, 1585-1601. 10.1016/j.ymthe.2020.12.019.
10. Banerjee, K., Nunez, F.J., Haase, S., McClellan, B.L., Faisal, S.M., Carney, S.V., Yu, J., Alghamri, M.S., Asad, A.S., Candia, A.J.N., et al. (2021). Current Approaches for Glioma Gene Therapy and Virotherapy. Front Mol Neurosci *14*, 621831. 10.3389/fnmol.2021.621831.
11. Noroozian, Z., Xhima, K., Huang, Y., Kaspar, B.K., Kugler, S., Hynynen, K., and Aubert, I. (2019). MRI-Guided Focused Ultrasound for Targeted Delivery of rAAV to the Brain. Methods Mol Biol *1950*, 177-197. 10.1007/978-1-4939-9139-6_10.
12. Rainov, N.G. (2000). A phase III clinical evaluation of herpes simplex virus type 1 thymidine kinase and ganciclovir gene therapy as an adjuvant to surgical resection and radiation in adults with previously untreated glioblastoma multiforme. Hum Gene Ther *11*, 2389-2401. 10.1089/104303400750038499.
13. Cloughesy, T.F., Petrecca, K., Walbert, T., Butowski, N., Salacz, M., Perry, J., Damek, D., Bota, D., Bettegowda, C., Zhu, J.J., et al. (2020). Effect of Vocimagene Amiretrorepvec in Combination With Flucytosine vs Standard of Care on Survival Following Tumor Resection in Patients With Recurrent High-Grade Glioma: A Randomized Clinical Trial. JAMA Oncol *6*, 1939-1946. 10.1001/jamaoncol.2020.3161.
14. Tamimi, A.F., and Juweid, M. (2017). Epidemiology and Outcome of Glioblastoma. In Glioblastoma, S. De Vleeschouwer, ed. 10.15586/codon.glioblastoma.2017.ch8.

15. Zanders, E.D., Svensson, F., and Bailey, D.S. (2019). Therapy for glioblastoma: is it working? Drug Discov Today *24*, 1193-1201. 10.1016/j.drudis.2019.03.008.
16. Kim, H.J., Park, J.W., and Lee, J.H. (2020). Genetic Architectures and Cell-of-Origin in Glioblastoma. Front Oncol *10*, 615400. 10.3389/fonc.2020.615400.
17. Kanu, O.O., Hughes, B., Di, C., Lin, N., Fu, J., Bigner, D.D., Yan, H., and Adamson, C. (2009). Glioblastoma Multiforme Oncogenomics and Signaling Pathways. Clin Med Oncol *3*, 39-52. 10.4137/cmo.s1008.
18. Aldape, K., Zadeh, G., Mansouri, S., Reifenberger, G., and von Deimling, A. (2015). Glioblastoma: pathology, molecular mechanisms and markers. Acta Neuropathol *129*, 829-848. 10.1007/s00401-015-1432-1.
19. Yang, J., Yan, J., and Liu, B. (2017). Targeting EGFRvIII for glioblastoma multiforme. Cancer Lett *403*, 224-230. 10.1016/j.canlet.2017.06.024.
20. Roffey, S.E., and Litchfield, D.W. (2021). CK2 Regulation: Perspectives in 2021. Biomedicines *9*. 10.3390/biomedicines9101361.
21. Borgo, C., D'Amore, C., Sarno, S., Salvi, M., and Ruzzene, M. (2021). Protein kinase CK2: a potential therapeutic target for diverse human diseases. Signal Transduct Target Ther *6*, 183. 10.1038/s41392-021-00567-7.
22. Venerando, A., Ruzzene, M., and Pinna, L.A. (2014). Casein kinase: the triple meaning of a misnomer. Biochem J *460*, 141-156. 10.1042/BJ20140178.
23. Goel, R.K., Meyer, M., Paczkowska, M., Reimand, J., Vizeacoumar, F., Vizeacoumar, F., Lam, T.T., and Lukong, K.E. (2018). Global phosphoproteomic analysis identifies SRMS-regulated secondary signaling intermediates. Proteome Sci *16*, 16. 10.1186/s12953-018-0143-7.
24. Lee, Y.H., Park, J.W., and Bae, Y.S. (2016). Regulation of protein kinase CK2 catalytic activity by protein kinase C and phospholipase D2. Biochimie *121*, 131-139. 10.1016/j.biochi.2015.12.005.
25. Chua, M.M., Ortega, C.E., Sheikh, A., Lee, M., Abdul-Rassoul, H., Hartshorn, K.L., and Dominguez, I. (2017). CK2 in Cancer: Cellular and Biochemical Mechanisms and Potential Therapeutic Target. Pharmaceuticals (Basel) *10*. 10.3390/ph10010018.
26. Zheng, Y., McFarland, B.C., Drygin, D., Yu, H., Bellis, S.L., Kim, H., Bredel, M., and Benveniste, E.N. (2013). Targeting protein kinase CK2 suppresses prosurvival signaling pathways and growth of glioblastoma. Clin Cancer Res *19*, 6484-6494. 10.1158/1078-0432.CCR-13-0265.
27. Halloran, D., Pandit, V., and Nohe, A. (2022). The Role of Protein Kinase CK2 in Development and Disease Progression: A Critical Review. J Dev Biol *10*. 10.3390/jdb10030031.
28. Meggio, F., and Pinna, L.A. (2003). One-thousand-and-one substrates of protein kinase CK2? FASEB J *17*, 349-368. 10.1096/fj.02-0473rev.
29. Borgo, C., and Ruzzene, M. (2019). Role of protein kinase CK2 in antitumor drug resistance. J Exp Clin Cancer Res *38*, 287. 10.1186/s13046-019-1292-y.
30. Ahmad, K.A., Wang, G., Unger, G., Slaton, J., and Ahmed, K. (2008). Protein kinase CK2--a key suppressor of apoptosis. Adv Enzyme Regul *48*, 179-187. 10.1016/j.advenzreg.2008.04.002.
31. Zakharia, K., Miyabe, K., Wang, Y., Wu, D., Moser, C.D., Borad, M.J., and Roberts, L.R. (2019). Preclinical In Vitro and In Vivo Evidence of an Antitumor Effect of CX-4945, a Casein Kinase II Inhibitor, in Cholangiocarcinoma. Transl Oncol *12*, 143-153. 10.1016/j.tranon.2018.09.005.
32. Siddiqui-Jain, A., Bliesath, J., Macalino, D., Omori, M., Huser, N., Streiner, N., Ho, C.B., Anderes, K., Proffitt, C., O'Brien, S.E., et al. (2012). CK2 inhibitor CX-4945 suppresses DNA repair response triggered by DNA-targeted anticancer drugs and augments efficacy:

mechanistic rationale for drug combination therapy. Mol Cancer Ther *11*, 994-1005. 10.1158/1535-7163.MCT-11-0613.
33. Ferrer-Font, L., Villamanan, L., Arias-Ramos, N., Vilardell, J., Plana, M., Ruzzene, M., Pinna, L.A., Itarte, E., Arus, C., and Candiota, A.P. (2017). Targeting Protein Kinase CK2: Evaluating CX-4945 Potential for GL261 Glioblastoma Therapy in Immunocompetent Mice. Pharmaceuticals (Basel) *10*. 10.3390/ph10010024.
34. Liu, X., Chen, J., Li, W., Hang, C., and Dai, Y. (2020). Inhibition of Casein Kinase II by CX-4945, But Not Yes-associated protein (YAP) by Verteporfin, Enhances the Antitumor Efficacy of Temozolomide in Glioblastoma. Transl Oncol *13*, 70-78. 10.1016/j.tranon.2019.09.006.
35. Lutz, S., and Iamurri, S.M. (2018). Protein Engineering: Past, Present, and Future. Methods Mol Biol *1685*, 1-12. 10.1007/978-1-4939-7366-8_1.
36. Sequeiros-Borja, C.E., Surpeta, B., and Brezovsky, J. (2021). Recent advances in user-friendly computational tools to engineer protein function. Brief Bioinform *22*. ARTN bbaa15010.1093/bib/bbaa150.
37. Tobin, P.H., Richards, D.H., Callender, R.A., and Wilson, C.J. (2014). Protein engineering: a new frontier for biological therapeutics. Curr Drug Metab *15*, 743-756. 10.2174/1389200216666141208151524.
38. Silva, D.A., Yu, S., Ulge, U.Y., Spangler, J.B., Jude, K.M., Labao-Almeida, C., Ali, L.R., Quijano-Rubio, A., Ruterbusch, M., Leung, I., et al. (2019). De novo design of potent and selective mimics of IL-2 and IL-15. Nature *565*, 186-191. 10.1038/s41586-018-0830-7.
39. Ebrahimi, S.B., and Samanta, D. (2023). Engineering protein-based therapeutics through structural and chemical design. Nat Commun *14*, 2411. 10.1038/s41467-023-38039-x.
40. Pearce, R., and Zhang, Y. (2021). Toward the solution of the protein structure prediction problem. J Biol Chem *297*, 100870. 10.1016/j.jbc.2021.100870.
41. Kuhlman, B., and Bradley, P. (2019). Advances in protein structure prediction and design. Nat Rev Mol Cell Biol *20*, 681-697. 10.1038/s41580-019-0163-x.
42. Jumper, J., Evans, R., Pritzel, A., Green, T., Figurnov, M., Ronneberger, O., Tunyasuvunakool, K., Bates, R., Zidek, A., Potapenko, A., et al. (2021). Highly accurate protein structure prediction with AlphaFold. Nature *596*, 583-589. 10.1038/s41586-021-03819-2.
43. Ruff, K.M., and Pappu, R.V. (2021). AlphaFold and Implications for Intrinsically Disordered Proteins. J Mol Biol *433*, 167208. 10.1016/j.jmb.2021.167208.
44. Laurents, D.V. (2022). AlphaFold 2 and NMR Spectroscopy: Partners to Understand Protein Structure, Dynamics and Function. Front Mol Biosci *9*, 906437. 10.3389/fmolb.2022.906437.
45. Uversky, V.N. (2016). Dancing Protein Clouds: The Strange Biology and Chaotic Physics of Intrinsically Disordered Proteins. J Biol Chem *291*, 6681-6688. 10.1074/jbc.R115.685859.
46. Trivedi, R., and Nagarajaram, H.A. (2022). Intrinsically Disordered Proteins: An Overview. Int J Mol Sci *23*. 10.3390/ijms232214050.
47. Day, E.K., Sosale, N.G., and Lazzara, M.J. (2016). Cell signaling regulation by protein phosphorylation: a multivariate, heterogeneous, and context-dependent process. Curr Opin Biotechnol *40*, 185-192. 10.1016/j.copbio.2016.06.005.
48. Esmaili, F., Pourmirzaei, M., Ramazi, S., Shojaeilangari, S., and Yavari, E. (2023). A Review of Machine Learning and Algorithmic Methods for Protein Phosphorylation Sites Prediction. Genomics Proteomics Bioinformatics. 10.1016/j.gpb.2023.03.007.

49. Jamal, S., Ali, W., Nagpal, P., Grover, A., and Grover, S. (2021). Predicting phosphorylation sites using machine learning by integrating the sequence, structure, and functional information of proteins. J Transl Med *19*, 218. 10.1186/s12967-021-02851-0.
50. Needham, E.J., Parker, B.L., Burykin, T., James, D.E., and Humphrey, S.J. (2019). Illuminating the dark phosphoproteome. Sci Signal *12*. 10.1126/scisignal.aau8645.
51. Johnson, J.L., Yaron, T.M., Huntsman, E.M., Kerelsky, A., Song, J., Regev, A., Lin, T.Y., Liberatore, K., Cizin, D.M., Cohen, B.M., et al. (2023). An atlas of substrate specificities for the human serine/threonine kinome. Nature *613*, 759-766. 10.1038/s41586-022-05575-3.
52. Soucheray, M., Capelletti, M., Pulido, I., Kuang, Y., Paweletz, C.P., Becker, J.H., Kikuchi, E., Xu, C., Patel, T.B., Al-Shahrour, F., et al. (2015). Intratumoral Heterogeneity in EGFR-Mutant NSCLC Results in Divergent Resistance Mechanisms in Response to EGFR Tyrosine Kinase Inhibition. Cancer Res *75*, 4372-4383. 10.1158/0008-5472.CAN-15-0377.
53. Engelman, J.A., and Janne, P.A. (2008). Mechanisms of acquired resistance to epidermal growth factor receptor tyrosine kinase inhibitors in non-small cell lung cancer. Clin Cancer Res *14*, 2895-2899. 10.1158/1078-0432.CCR-07-2248.
54. Engelman, J.A., Zejnullahu, K., Mitsudomi, T., Song, Y., Hyland, C., Park, J.O., Lindeman, N., Gale, C.M., Zhao, X., Christensen, J., et al. (2007). MET amplification leads to gefitinib resistance in lung cancer by activating ERBB3 signaling. Science *316*, 1039-1043. 10.1126/science.1141478.
55. Greco, O., and Dachs, G.U. (2001). Gene directed enzyme/prodrug therapy of cancer: historical appraisal and future prospectives. J Cell Physiol *187*, 22-36. 10.1002/1097-4652(2001)9999:9999<::AID-JCP1060>3.0.CO;2-H.
56. Saukkonen, K., and Hemminki, A. (2004). Tissue-specific promoters for cancer gene therapy. Expert Opin Biol Ther *4*, 683-696. 10.1517/14712598.4.5.683.
57. Robson, T., and Hirst, D.G. (2003). Transcriptional Targeting in Cancer Gene Therapy. J Biomed Biotechnol *2003*, 110-137. 10.1155/S1110724303209074.
58. van Dillen, I.J., Mulder, N.H., Vaalburg, W., de Vries, E.F., and Hospers, G.A. (2002). Influence of the bystander effect on HSV-tk/GCV gene therapy. A review. Curr Gene Ther *2*, 307-322. 10.2174/1566523023347733.
59. Tanaka, T., Duflot-Dancer, A., Tiraby, M., Piccoli, C., Tiraby, G., Yamasaki, H., and Mesnil, M. (2009). Bystander effect from cytosine deaminase and uracil phosphoribosyl transferase genes in vitro: a partial contribution of gap junctions. Cancer Lett *282*, 43-47. 10.1016/j.canlet.2009.02.050.
60. Albeck, J.G., Mills, G.B., and Brugge, J.S. (2013). Frequency-modulated pulses of ERK activity transmit quantitative proliferation signals. Mol Cell *49*, 249-261. 10.1016/j.molcel.2012.11.002.
61. Basbous, J., Chalbos, D., Hipskind, R., Jariel-Encontre, I., and Piechaczyk, M. (2007). Ubiquitin-independent proteasomal degradation of Fra-1 is antagonized by Erk1/2 pathway-mediated phosphorylation of a unique C-terminal destabilizer. Mol Cell Biol *27*, 3936-3950. 10.1128/MCB.01776-06.
62. Rechsteiner, M. (1990). PEST sequences are signals for rapid intracellular proteolysis. Semin Cell Biol *1*, 433-440.
63. Rechsteiner, M., and Rogers, S.W. (1996). PEST sequences and regulation by proteolysis. Trends Biochem Sci *21*, 267-271.
64. Correa Marrero, M., van Dijk, A.D.J., and de Ridder, D. (2017). Sequence-based analysis of protein degradation rates. Proteins *85*, 1593-1601. 10.1002/prot.25323.
65. Guharoy, M., Lazar, T., Macossay-Castillo, M., and Tompa, P. (2022). Degron masking outlines degronons, co-degrading functional modules in the proteome. Commun Biol *5*, 445. 10.1038/s42003-022-03391-z.

66. Hornbeck, P.V., Kornhauser, J.M., Tkachev, S., Zhang, B., Skrzypek, E., Murray, B., Latham, V., and Sullivan, M. (2012). PhosphoSitePlus: a comprehensive resource for investigating the structure and function of experimentally determined post-translational modifications in man and mouse. Nucleic Acids Res *40*, D261-270. 10.1093/nar/gkr1122.
67. Wilkins, M.R., Gasteiger, E., Bairoch, A., Sanchez, J.C., Williams, K.L., Appel, R.D., and Hochstrasser, D.F. (1999). Protein identification and analysis tools in the ExPASy server. Methods Mol Biol *112*, 531-552. 10.1385/1-59259-584-7:531.
68. Belizario, J.E., Alves, J., Garay-Malpartida, M., and Occhiucci, J.M. (2008). Coupling caspase cleavage and proteasomal degradation of proteins carrying PEST motif. Curr Protein Pept Sci *9*, 210-220. 10.2174/138920308784534023.
69. Borgo, C., D'Amore, C., Cesaro, L., Itami, K., Hirota, T., Salvi, M., and Pinna, L.A. (2020). A N-terminally deleted form of the CK2alpha' catalytic subunit is sufficient to support cell viability. Biochem Biophys Res Commun *531*, 409-415. 10.1016/j.bbrc.2020.07.112.
70. Di Maira, G., Salvi, M., Arrigoni, G., Marin, O., Sarno, S., Brustolon, F., Pinna, L.A., and Ruzzene, M. (2005). Protein kinase CK2 phosphorylates and upregulates Akt/PKB. Cell Death Differ *12*, 668-677. 10.1038/sj.cdd.4401604.
71. Duarte, D., and Vale, N. (2022). Evaluation of synergism in drug combinations and reference models for future orientations in oncology. Curr Res Pharmacol Drug Discov *3*, 100110. 10.1016/j.crphar.2022.100110.
72. Wright, R.C., Khakhar, A., Eshleman, J.R., and Ostermeier, M. (2014). Advancements in the development of HIF-1alpha-activated protein switches for use in enzyme prodrug therapy. PLoS One *9*, e114032. 10.1371/journal.pone.0114032.
73. Joosten, R.P., and Agirre, J. (2022). Whole-proteome structures shed new light on posttranslational modifications. PLoS Biol *20*, e3001673. 10.1371/journal.pbio.3001673.
74. Okazaki, K., and Sagata, N. (1995). The Mos/MAP kinase pathway stabilizes c-Fos by phosphorylation and augments its transforming activity in NIH 3T3 cells. EMBO J *14*, 5048-5059. 10.1002/j.1460-2075.1995.tb00187.x.
75. Terasawa, K., Okazaki, K., and Nishida, E. (2003). Regulation of c-Fos and Fra-1 by the MEK5-ERK5 pathway. Genes Cells *8*, 263-273. 10.1046/j.1365-2443.2003.00631.x.
76. Hu, T.T., and Luo, S.Z. (2011). Phosphorylation-Induced Structural Changes in the C-Terminus of c-Fos Detected by CD and NMR. Int J Pept Res Ther *17*, 19-30. 10.1007/s10989-010-9236-6.
77. van, I.D.G.P., Forghany, Z., Liebelt, F., Vertegaal, A.C., Jochemsen, A.G., Bovee, J., Szuhai, K., and Baker, D.A. (2017). Functional analyses of a human vascular tumor FOS variant identify a novel degradation mechanism and a link to tumorigenesis. J Biol Chem *292*, 21282-21290. 10.1074/jbc.C117.815845.
78. Hendus-Altenburger, R., Lambrughi, M., Terkelsen, T., Pedersen, S.F., Papaleo, E., Lindorff-Larsen, K., and Kragelund, B.B. (2017). A phosphorylation-motif for tuneable helix stabilisation in intrinsically disordered proteins - Lessons from the sodium proton exchanger 1 (NHE1). Cell Signal *37*, 40-51. 10.1016/j.cellsig.2017.05.015.
79. Jin, C., Song, P., and Pang, J. (2019). The CK2 inhibitor CX4945 reverses cisplatin resistance in the A549/DDP human lung adenocarcinoma cell line. Oncol Lett *18*, 3845-3856. 10.3892/ol.2019.10696.
80. Yang, B., Yao, J., Li, B., Shao, G., and Cui, Y. (2017). Inhibition of protein kinase CK2 sensitizes non-small cell lung cancer cells to cisplatin via upregulation of PML. Mol Cell Biochem *436*, 87-97. 10.1007/s11010-017-3081-2.
81. Kalathur, M., Toso, A., Chen, J., Revandkar, A., Danzer-Baltzer, C., Guccini, I., Alajati, A., Sarti, M., Pinton, S., Brambilla, L., et al. (2015). A chemogenomic screening identifies CK2 as a target for pro-senescence therapy in PTEN-deficient tumours. Nat Commun *6*, 7227. 10.1038/ncomms8227.

82. Sheng, W.J., Jiang, H., Wu, D.L., and Zheng, J.H. (2013). Early responses of the STAT3 pathway to platinum drugs are associated with cisplatin resistance in epithelial ovarian cancer. Braz J Med Biol Res *46*, 650-658. 10.1590/1414-431X20133003.
83. Li, D.M., and Sun, H. (1998). PTEN/MMAC1/TEP1 suppresses the tumorigenicity and induces G1 cell cycle arrest in human glioblastoma cells. Proc Natl Acad Sci U S A *95*, 15406-15411. 10.1073/pnas.95.26.15406.
84. Li, J., Yen, C., Liaw, D., Podsypanina, K., Bose, S., Wang, S.I., Puc, J., Miliaresis, C., Rodgers, L., McCombie, R., et al. (1997). PTEN, a putative protein tyrosine phosphatase gene mutated in human brain, breast, and prostate cancer. Science *275*, 1943-1947. 10.1126/science.275.5308.1943.
85. Lee, E.S., Ko, K.K., Joe, Y.A., Kang, S.G., and Hong, Y.K. (2011). Inhibition of STAT3 reverses drug resistance acquired in temozolomide-resistant human glioma cells. Oncol Lett *2*, 115-121. 10.3892/ol.2010.210.
86. Bibby, A.C., and Litchfield, D.W. (2005). The multiple personalities of the regulatory subunit of protein kinase CK2: CK2 dependent and CK2 independent roles reveal a secret identity for CK2beta. Int J Biol Sci *1*, 67-79. 10.7150/ijbs.1.67.
87. Pinna, L.A. (2002). Protein kinase CK2: a challenge to canons. J Cell Sci *115*, 3873-3878. 10.1242/jcs.00074.
88. Schmidt-Spaniol, I., Grimm, B., and Issinger, O.G. (1993). Subcellular localization of protein kinase CK-2 alpha- and beta-subunits in synchronized cells from primary human fibroblasts and established cell lines. Cell Mol Biol Res *39*, 761-772.
89. Wainstein, E., Maik-Rachline, G., Blenis, J., and Seger, R. (2022). AKTs do not translocate to the nucleus upon stimulation but AKT3 can constitutively signal from the nuclear envelope. Cell Rep *41*, 111733. 10.1016/j.celrep.2022.111733.
90. Girardi, C., James, P., Zanin, S., Pinna, L.A., and Ruzzene, M. (2014). Differential phosphorylation of Akt1 and Akt2 by protein kinase CK2 may account for isoform specific functions. Biochim Biophys Acta *1843*, 1865-1874. 10.1016/j.bbamcr.2014.04.020.
91. Schulz, J.A., Rodgers, L.T., Kryscio, R.J., Hartz, A.M.S., and Bauer, B. (2022). Characterization and comparison of human glioblastoma models. BMC Cancer *22*, 844. 10.1186/s12885-022-09910-9.
92. Brighi, C., Reid, L., Genovesi, L.A., Kojic, M., Millar, A., Bruce, Z., White, A.L., Day, B.W., Rose, S., Whittaker, A.K., and Puttick, S. (2020). Comparative study of preclinical mouse models of high-grade glioma for nanomedicine research: the importance of reproducing blood-brain barrier heterogeneity. Theranostics *10*, 6361-6371. 10.7150/thno.46468.
93. Pakay, J.L., Diesch, J., Gilan, O., Yip, Y.Y., Sayan, E., Kolch, W., Mariadason, J.M., Hannan, R.D., Tulchinsky, E., and Dhillon, A.S. (2012). A 19S proteasomal subunit cooperates with an ERK MAPK-regulated degron to regulate accumulation of Fra-1 in tumour cells. Oncogene *31*, 1817-1824. 10.1038/onc.2011.375.
94. Garcia-Alai, M.M., Gallo, M., Salame, M., Wetzler, D.E., McBride, A.A., Paci, M., Cicero, D.O., and de Prat-Gay, G. (2006). Molecular basis for phosphorylation-dependent, PEST-mediated protein turnover. Structure *14*, 309-319. 10.1016/j.str.2005.11.012.